Identification of Novel Kinases of Tau Using Fluorescence Complementation Mass Spectrometry (FCMS)†

Authors

Der-Shyang Kao, Yanyan Du, Andrew G. DeMarco, Sehong Min, Mark C. Hall, Jean-Christophe Rochet, and W. Andy Tao

Correspondence

taow@purdue.edu

In Brief

Tau hyperphosphorylation has been associated with Alzheimer's disease, and identification of unknown Tau kinases is essential. Here, we uncovered novel kinase candidates of Tau using fluorescence complementation mass spectrometry. *In vitro* phosphorylation validated that OXSR1, DAPK2, CSK, and ZAP70 can directly phosphorylate Tau. Cotransduction of Tau and each of these four kinases could increase Tau phosphorylation in H4 cells.

Graphical Abstract

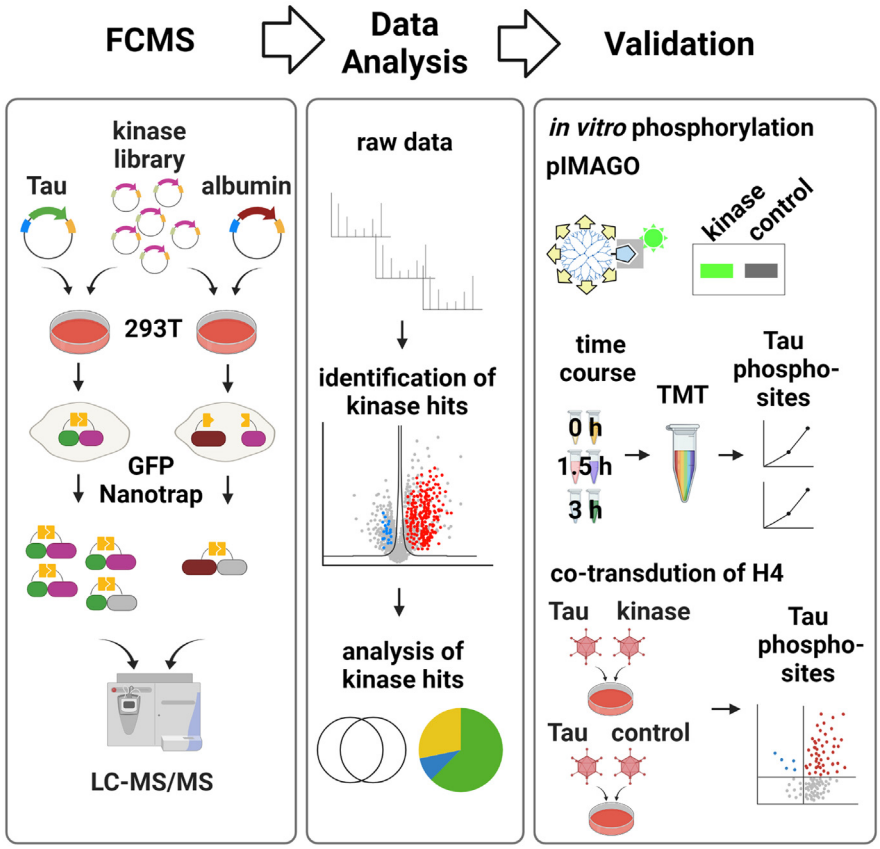

Highlights

- Fluorescence complementation mass spectrometry allowed us to systematically identify the kinases that can phosphorylate Tau.
- Thirty-six kinases without prior knowledge of phosphorylating Tau were identified.
- *In vitro* kinase assay and tandem mass tag labeling validated four kinases and phosphorylation sites on Tau.
- Cotransduction of Tau and each kinase increased Tau phosphorylation in H4 cells.

2022, Mol Cell Proteomics *21*(*12*), 100441

https://doi.org/10.1016/j.mcpro.2022.100441

Identification of Novel Kinases of Tau Using Fluorescence Complementation Mass Spectrometry (FCMS)†

Der-Shyang Kao[1], Yanyan Du[1], Andrew G. DeMarco[1], Sehong Min[2], Mark C. Hall[1,3], Jean-Christophe Rochet[2,4], and W. Andy Tao[1,2,3,5,*]

Hyperphosphorylation of the microtubule-associated protein Tau is a major hallmark of Alzheimer's disease and other tauopathies. Understanding the protein kinases that phosphorylate Tau is critical for the development of new drugs that target Tau phosphorylation. At present, the repertoire of the Tau kinases remains incomplete, and methods to uncover novel upstream protein kinases are still limited. Here, we apply our newly developed proteomic strategy, fluorescence complementation mass spectrometry, to identify novel kinase candidates of Tau. By constructing Tau- and kinase-fluorescent fragment library, we detected 59 Tau-associated kinases, including 23 known kinases of Tau and 36 novel candidate kinases. In the validation phase using *in vitro* phosphorylation, among 15 candidate kinases we attempted to purify and test, four candidate kinases, OXSR1 (oxidative-stress responsive gene 1), DAPK2 (death-associated protein kinase 2), CSK (C-terminal SRC kinase), and ZAP70 (zeta chain of T-cell receptor–associated protein kinase 70), displayed the ability to phosphorylate Tau in time-course experiments. Furthermore, coexpression of these four kinases along with Tau increased the phosphorylation of Tau in human neuroglioma H4 cells. We demonstrate that fluorescence complementation mass spectrometry is a powerful proteomic strategy to systematically identify potential kinases that can phosphorylate Tau in cells. Our discovery of new candidate kinases of Tau can present new opportunities for developing Alzheimer's disease therapeutic strategies.

Alzheimer's disease (AD) is the most predominant dementia disease, causing substantial social and economic impacts. It has been estimated to account for 60% to 80% of dementia cases worldwide (1). The prevalence of AD is predicted to increase dramatically in the 21st century. However, efficient treatments are still rarely available to date (2, 3). In AD, neurofibrillary tangles (NFTs) have been characterized as one of the major disease hallmarks, which are primarily composed of paired helical filaments (4, 5). Paired helical filaments primarily consist of hyperphosphorylated forms of Tau, a microtubule-associated protein that stabilizes the cytoskeleton in neurons. The interaction between Tau and microtubule can be regulated by phosphorylation of Tau. The phosphorylation of several phosphosites of Tau has been reported to result in a change in the protein's conformation, eventually altering its binding affinity for microtubules and inducing protein aggregation (6–8). There has been accumulating evidence strongly indicating that the hyperphosphorylation of Tau is a critical AD pathogenic event as well as a key AD biomarker (2, 3). Other studies have revealed that similar abnormal phosphorylation of Tau is also involved in the pathomechanism of other neurodegenerative disorders, which together with AD are called tauopathies (4). In mouse models, the inactivation of Tau kinases has been reported to improve neurodegenerative phenotypes (9, 10). Therefore, inhibiting the Tau kinases, the enzymes that phosphorylate Tau, has been proposed to be a promising therapeutic strategy to reduce the hyperphosphorylation of Tau and ultimately prevent the development of tauopathies. Identifying the kinases and kinase networks involved in Tau hyperphosphorylation is a major priority in current research on neurodegenerative diseases (4, 11).

However, despite tremendous endeavors to uncover the Tau kinases for decades, the knowledge of these kinases is still limited. Tau is a highly intricate phosphoprotein. A notable characteristic of Tau is its high number of phosphosites. The longest isoform of Tau in the human adult brain (2N4R) has 85 possible phosphorylation sites (45 serine residues, 35 threonine residues, and 5 tyrosine residues), representing one of the most complex phosphoproteins (4). There are still five phosphosites for which no kinases have yet been identified, implying that there may be undiscovered kinases of Tau (4, 5,

From the [1]Department of Biochemistry, [2]Department of Medicinal Chemistry and Molecular Pharmacology, [3]Purdue Center for Cancer Research, [4]Purdue Institute for Integrative Neuroscience, and [5]Department of Chemistry, Purdue University, West Lafayette, Indiana, USA
*For correspondence: W. Andy Tao, taow@purdue.edu.
†In memory of Dr Chang-Deng Hu, the co-inventor of bimolecular fluorescence complementation.

https://doi.org/10.1016/j.mcpro.2022.100441

12–14) (table of tau phosphorylation sites; https://bit.ly/2JyZTbS). Although the functions of these five phosphosites have not yet been fully characterized, the phosphorylation of three of these uncharacterized sites was detected in AD postmortem brains (15), suggesting possible significance of these phosphorylated sites in the development of AD. Thus, it is necessary to reveal the missing information, and searching for unidentified kinases of Tau is essential to solve this problem.

Moreover, there are no clinically approved drugs of the known Tau kinases. These kinase targets include the well-characterized Tau kinases GSK3 and Fyn. Despite massive development efforts, none of these drug candidates has been proven to show significant clinical benefits (16). In fact, many phosphosites, including those primarily observed in post-mortem AD brains, are already known to be phosphorylated by multiple kinases (4, 12–14). These observations strongly suggest that many Tau kinases have not yet been identified and characterized as the inhibition of the activities of known kinases may be compensated by unknown kinases. The discovery of these unknown kinases of Tau is indispensable for developing new therapeutic agents for tauopathies.

Unfortunately, systematic approaches to identify upstream kinases of a specific substrate are still limited. This situation hampers our ability to discover unidentified kinases to understand the diseases related to dysregulated phosphorylation. It has been attempted to capture potential interacting kinases by affinity pull-down or coimmunoprecipitation (co-IP) using an immobilized substrate (17, 18). However, this strategy is impeded by the weak or transient interactions between kinases and their substrates. In a study aiming to identify kinases of Tau, kinases were transfected into human neuroblastoma cells, and the kinases resulting in higher phosphorylation levels of Tau were considered candidate kinases (19). However, only five phosphorylation sites were measured in this work. Therefore, kinases that phosphorylate other critical sites could be missed. In addition, this approach could not distinguish the difference between direct and indirect phosphorylation by the tested kinases.

To overcome the current hindrance, our group has recently developed a novel approach, fluorescence complementation mass spectrometry (FCMS) (20). FCMS takes the advantages of Venus fluorescent protein fragments (VN155 and VC155) in the bimolecular fluorescence complementation (BiFC) method, which form a stable VN155–VC155 fluorescent complex *in vivo* (21). In this method, a substrate and a kinase library are fused with VN155 and VC155, respectively, and weak kinase–substrate interactions can be fixed by the stable VN155–VC155 fluorescent complex in cells. Hence, the weak kinase–substrate complexes can be stabilized to facilitate specific isolation by GFP nanobody for subsequent LC–MS identification. This method can break through the conventional limitation of co-IP for identifying transiently interacting kinases. In this study, it is the first time we have applied this novel method to unveil novel kinases that are potentially involved in neurodegenerative diseases. We aimed to use FCMS to uncover novel kinase candidates of Tau in a high-throughput manner and then validate these kinase candidates using *in vitro* phosphorylation assays and in a human neuroglioma cell line.

EXPERIMENTAL PROCEDURES

Cell Culture

Human embryonic kidney (HEK) 293T and 293A cells and human neuroglioma H4 cells were purchased from American Type Culture Collection and cultured in Dulbecco's modified essential medium (Corning) supplemented with 10% heat inactivated fetal bovine serum (Corning) at 37 °C in 5% CO_2 (v/v).

Generation of the Human Kinase Library

The human kinase expression clones were generated using the Gateway technique. The human kinase ORF plasmid collection kit was purchased from Addgene (Addgene kit; #1000000014, contributed by William Hahn and David Root). The kit consists of 559 distinct human kinases and kinase-related protein ORFs in pDONR-223 Gateway Entry vectors. DNA encoding attR1–ccdB–attR2 was cloned in frame into the EcoRI/XhoI sites of pHA-MCS-2(4G1S)Linker-VC155(A206K) to generate the destination vector. Then, the LR reaction was performed, and expression clones encoding hemagglutinin (HA)-kinase-VC155 were generated. The 559 clones were stored separately in *Escherichia coli* DH5α at –80 °C. To prepare the expression library, the 559 *E. coli* DH5α cultures carrying distinct HA-kinase-VC155 expression clones were grown separately, pooled, and then the plasmids were extracted. To generate the Tau 2N4R expression clone and the albumin expression clone, complementary DNAs (cDNAs) encoding Tau 2N4R and albumin were amplified by PCR using DNA constructs encoding Tau 2N4R and albumin ORF as the templates. The amplified cDNAs were then cloned in frame into the EcoRI/XhoI sites of pMyc-MCS-2(4G1S)Linker-VN155(I152L).

Cell Transfection, Cell Lysis, and Immunoprecipitation

Cells grown to approximately 60% confluency were transfected with plasmids encoding Tau and the human kinase library generated in this study using Lipofectamine 2000 Reagent (Life Technologies) and Opti-MEM (Gibco). The cell culture medium was replaced the next day, and after a 48 h incubation period to allow for protein expression, the cells were trypsinized and collected by centrifugation. Cells were washed with ice-cold PBS once, then lysed in 0.4 ml of lysis buffer (50 mM Tris–HCl, pH 7.5, 150 mM NaCl, 1% NP-40) supplemented with protease inhibitor cocktail (Pierce) by sonication. After centrifugation of the lysate at the maximal speed for 30 min at 4 °C, the lysate supernatant was recovered, diluted to 1 ml with wash buffer (50 mM Tris–Cl [pH 7.5] and 150 mM NaCl) supplemented with protease inhibitor cocktail, and subjected to immunoprecipitation [IP] with GFP-Trap Magnetic Agarose beads (ChromoTek) for 1 h at 4 °C. Bead-bounded protein complexes were washed once with lysis buffer, once with radioimmunoprecipitation assay buffer (50 mM Tris–Cl [pH 7.5]; 150 mM NaCl; 0.5 mM EDTA; 0.1% SDS; 1% Triton X-100; and 1% deoxycholate), and once with wash buffer.

Preparation of FCMS Immunoprecipitated and Tandem Mass Tag–Labeled Samples for Mass Spectrometry

The GFP-Trap bead-bound protein complexes were denatured, reduced, and alkylated in the phase transfer surfactant–aided buffer

(12 mM sodium deoxycholate, 12 mM sodium lauroyl sarcosinate, 10 mM Tris(2-carboxyethyl)phosphine, and 40 mM chloroacetamide) at 95 °C for 5 min. The denatured, reduced, and alkylated protein samples were diluted fivefold with 50 mM triethylammonium bicarbonate (TEAB) and then digested with proteomics grade trypsin (Sigma) at a final enzyme-to-protein ratio of 1:50 (w/w) overnight at 37 °C. The peptide samples were cleaned up by adding the same volume of ethyl acetate and vortexing to remove sodium deoxycholate and sodium lauroyl sarcosinate. Then, the peptide samples were desalted by SDB-XC (3M Empore). Peptide eluents were vacuum dried. Peptide amounts were quantified using Thermo Scientific Pierce Quantitative Peptide Assays & Standards (catalog number: 23275).

For tandem mass tag (TMT)–labeled samples, the samples were denatured in 8 M urea, reduced by incubating with DTT at 37 °C for 30 min, and alkylated by treating with iodoacetamide at room temperature for 1 h. The samples were diluted fivefold with 50 mM TEAB and then digested with Lys-C (Wako) at a 1:100 (w/w) enzyme-to-protein ratio for 3 h at 37 °C. Trypsin was added to a final enzyme-to-protein ratio of 1:50 (w/w) for overnight digestion at 37 °C. The peptide samples were desalted by SDB-XC (3M Empore). Peptide eluents were vacuum dried. Peptide amounts were quantified using Thermo Scientific Pierce Quantitative Peptide Assays & Standards (catalog number: 23275).

Mass Spectrometric Data Acquisition

For mass spectrometric analyses on the LTQ-Orbitrap Velos Pro (Thermo Fisher Scientific), dried peptide samples were dissolved in 4.5 μl of 0.1% formic acid and 4 μl of each sample was injected into the EASY-nLC 1000 Liquid Chromatograph (Thermo Fisher Scientific). The reverse-phase separation was performed using an in-house C18 capillary column packed with 3 μm C18 bead resin (Michrom). The mobile phase buffer consisted of 0.1% formic acid in ultrapure water with the elution buffer of 0.1% formic acid in 80% CH_3CN run over a shallow linear gradient (from 2% CH_3CN to 40% CH_3CN) over 120 min with a flow rate of 200 nl/min. The EASY-nLC 1000 Liquid Chromatograph system was coupled online with a hybrid linear ion trap Orbitrap mass spectrometer (LTQ-Orbitrap Velos Pro; Thermo Fisher Scientific). The mass spectrometer was operated in the data-dependent mode in which a full-scan mass spectrometry (MS) (from *m/z* 300 to 1700 with a resolution of 30,000 at *m/z* 400) was followed by MS/MS of the top 20 most abundant ions from the full scan selected for collision-induced dissociation (35% energy), with MS/MS detection in the linear ion trap.

For quantitative analysis of TMT-labeled peptides using a Q-Exactive HF-X mass spectrometer (Thermo Fisher Scientific), dried peptide samples were dissolved in 10.8 μl of 0.05% trifluoroacetic acid with 3% (v/v) acetonitrile, and 10 μl of each sample was injected into an Ultimate 3000 Nano UHPLC system (Thermo Fisher Scientific). Peptides were captured on a 2 cm Acclaim PepMap trap column and separated on an in-house capillary column packed with 3 μm C18 bead resin. The mobile phase buffer consisted of 0.1% formic acid in ultrapure water (buffer A) with an eluting buffer of 0.1% formic acid in 80% (v/v) acetonitrile (buffer B) run with a linear 60 min gradient of 6 to 30% buffer B at a flow rate of 300 nl/min. The UHPLC was coupled online with a Q-Exactive HF-X mass spectrometer (Thermo Fisher Scientific) operated in the data-dependent mode, in which a full-scan MS (from *m/z* 375–1500 with a resolution of 60,000) was followed by MS/MS of the top 15 most intense ions (30,000 resolution; normalized collision energy = 8%; automatic gain control target = 2E4, maximum injection time = 200 ms; and 60 s exclusion).

LC–MS Data Processing

The LTQ-Orbitrap Velos Pro raw files were searched directly against the UniProt human protein database (downloaded on November 1, 2021; total number of entries: 20,531) using SEQUEST HT on Proteome Discoverer (version 2.2; Thermo Fisher Scientific). Searches were performed with full tryptic digestion and allowed a maximum of two missed cleavages on the peptides analyzed from the sequence database. Search criteria included a static carbamidomethylation of cysteine residues (+57.0214 Da) and a variable modification of oxidation of methionine residues (+15.9949 Da) and acetylation of protein N termini (+42.011 Da). MS1 peptide precursor mass tolerance was set at 10 ppm, and MS2 fragment mass tolerance was set at 0.6 Da. The false discovery rates (FDRs) of proteins and peptides were set at 1% for each analysis. All protein and peptide identifications were grouped, and any redundant entries were removed.

The Q-Exactive HF-X raw files were searched directly against the UniProt human protein database (downloaded on November 1, 2021; total number of entries: 20,531) using SEQUEST HT on Proteome Discoverer (version 2.3). Searches were performed with full tryptic digestion and allowed a maximum of two missed cleavages on the peptides analyzed from the sequence database. Search criteria included a static carbamidomethylation of cysteines (+57.0214 Da) and TMT 6-plex of lysine (+229.163 Da), and variable modifications of oxidation of methionine residues (+15.9949 Da), TMT 6-plex at peptide N termini (+229.163 Da), acetylation at protein N termini (+42.011 Da), and phosphorylation (+79.996 Da) on serine, threonine, or tyrosine residues. MS1 peptide precursor mass tolerance was set at 10 ppm, and MS2 fragment mass tolerance was set at 0.02 Da. The cutoff for co-isolation was 50%, and S/N was 10. The normalization mode in Reporter Ions Quantifier in the consensus workflow was set to be none. Proteome Discoverer created DTA files from raw data files with a minimum ion threshold of 15 and an absolute intensity threshold of 50. The FDRs of proteins and peptides were set at 0.01. All protein and peptide identifications were grouped, and any redundant entries were removed. Only unique peptides and unique master proteins were reported.

Quantification Analysis

All data were searched using SEQUEST HT and quantified using the label-free quantitation node of Precursor Ions Quantifier through the Proteome Discoverer (version 2.2 or 2.3). For the quantification of both proteomic and phosphoproteomic data, the intensities of peptides and phosphopeptides were extracted with the initial precursor mass tolerance set at 10 ppm, minimum number of isotope peaks as 2, maximum ΔRT of isotope pattern multiplets as 0.2 min, peptide-spectrum match confidence FDR of 0.01, with hypothesis test of ANOVA, maximum retention time shift of 5 min, pairwise ratio–based ratio calculation, and 100 as the maximum allowed fold change. Statistical analysis was performed in the Perseus software (22, 23) (version 1.6.5.0 or 1.6.15.0). Protein intensities were log2-transformed for analysis. All permutation-based *t* tests were two-sided and unpaired (FDR = 0.05, s0 = 0.2). For TMT experiments, the reporter ion intensities of unphosphorylated Tau peptides (without cognate phosphopeptides) were assumed to be constant in all samples and thus were used to normalize the reporter ion intensities within 6-plex experiments.

Bioinformatic Analysis

Kinase interaction network analyses were performed using STRING (24) (version 11.5). Only physical subnetworks (evidenced by text mining, experiments, and databases) were considered. Clustering analysis was performed with a Markov clustering inflation parameter of 3.

Protein Expression and Purification

To generate the Tau 2N4R expression construct, a cDNA encoding Tau 2N4R was amplified by PCR and subcloned in frame into the BamHI/XhoI sites of pET28b. *E. coli* BL21 (DE3) cells transformed with the resulting plasmid were induced to overexpress His-tagged Tau

2N4R and subsequently lysed *via* sonication in lysis buffer (50 mM monobasic sodium phosphate, 300 mM sodium chloride, 2 mM imidazole, pH 8.0) containing protease inhibitor cocktail. Extracts were cleared by centrifugation for 30 min at 4 °C at 20,627*g* and loaded onto a spin column containing nickel–nitrilotriacetic acid beads (Thermo Fisher Scientific). The column was washed with wash buffer 1 (50 mM monobasic sodium phosphate, 300 mM sodium chloride, 10 mM imidazole, pH 8.0) and wash buffer 2 (50 mM monobasic sodium phosphate, 300 mM sodium chloride, 25 mM imidazole, pH 8.0). His-tagged Tau was eluted with elution buffer (50 mM monobasic sodium phosphate, 300 mM sodium chloride, 500 mM imidazole, pH 8.0). The buffer was replaced with 50 mM Tris (pH 7.5) using an Amicon Ultra-15 Centrifugal Filter (Millipore).

Kinase candidates were purified from HEK293T cells harboring a plasmid encoding the HA-tagged kinases. Cells were lysed *via* sonication in ice-cold Tris-buffered saline supplemented with 0.1% Tween-20 (TBST; pH 7.4) and protease inhibitor cocktail. Extracts were cleared by centrifugation for 30 min at 4 °C at 20,627*g*. Anti-HA magnetic beads (Pierce) prewashed with TBST three times were added to the cell lysate, and the mixture was incubated for 3 h at 4 °C. The anti-HA magnetic beads were then washed with ice-cold TBST three times and then once more with 50 mM Tris (pH 7.5).

In Vitro *Phosphorylation Reactions and Phosphorylation Imaging (pIMAGO)*

The purified kinases on the anti-HA magnetic beads and the His-tagged Tau were mixed in a reaction buffer for *in vitro* phosphorylation reactions. The reaction buffer for each kinase was optimized according to the Assay Guidance Manual. The optimized kinase reaction buffer for OXSR1 (oxidative-stress responsive gene 1) is 50 mM Tris–HCl (pH 7.5), 500 μM ATP, 5 mM $MnCl_2$, and 1 mM DTT. The optimized kinase reaction buffer for DAPK2 (death-associated protein kinase 2) is 50 mM Tris–HCl (pH 7.5), 500 μM ATP, 5 mM $MgCl_2$, and 1 mM DTT. The optimized kinase reaction buffer for CSK (C-terminal SRC kinase) and ZAP70 (zeta chain of T-cell receptor–associated protein kinase 70) is 50 mM Tris–HCl (pH 7.5), 50 μM ATP, 20 mM $MgCl_2$, 5 mM $MnCl_2$, and 1 mM DTT. The *in vitro* phosphorylation reaction was carried out at 30 °C for 3 h. After the reaction, the anti-HA magnetic beads with bound kinases were removed by a magnetic rack.

Tau phosphoproteins generated in the *in vitro* phosphorylation reaction were analyzed *via* Western blotting using the phosphorylation imaging (pIMAGO)-biotin phosphoprotein detection system according to the product manual. Before running the gel, samples were boiled in LDS and DTT sample buffer at 95 °C for 5 min. Iodoacetamide was added to each sample to a final concentration of 0.5 for one time, and the mixture was incubated in the dark for 15 min at room temperature. The samples were loaded onto an SDS-PAGE gel and transferred to a membrane, which was then incubated with 1× blocking buffer followed by the pIMAGO reagent in 1× blocking buffer (1 h for each incubation). After washing the membrane three times with 1× wash buffer and once with 1× TBST (5 min each time), the membrane was incubated with avidin-Fluor in 1× blocking buffer for 1 h and then washed with TBST three times. pIMAGO images were developed in a fluorescence scanner.

In vitro *Time-Course Phosphorylation Reactions*

For the kinase time-course experiments, aliquots of *in vitro* phosphorylation samples were collected at 0, 1.5, and 3 h. After sample digestion and desalting, each sample was resuspended in 50 mM TEAB (pH 8.4) for 6-plex TMT labeling (Thermo Fisher Scientific). Samples were labeled in the following order: TMT126: kinase-present, 0 h; TMT127: kinase-present, 1.5 h; TMT128: kinase-present, 3 h; TMT129: kinase-null, 0 h; TMT130: kinase-null, 1.5 h; and TMT131: kinase-null, 3 h. Data normalization was conducted using unphosphorylated Tau peptides (without cognate phosphopeptides), which were assumed to have the same concentration in all samples.

Preparation of Adenoviral Constructs for Protein Expression in H4 Cells

Adenoviruses encoding Tau 2N4R with an N-terminal 3xFLAG tag and four of the kinases identified *via* proteomic analysis during the first phase of the study (CSK, DAPK2, OXSR1, and ZAP70), each with an N-terminal HA tag, were prepared using the ViraPower Adenoviral Expression System (Invitrogen). Briefly, cDNAs encoding 3xFLAG-Tau 2N4R and the HA-kinases were subcloned into the entry vector pENTR1A using the NEB HiFi kit (New England Biolabs). Inserts from the pENTR1A constructs were transferred to the destination vector pAD/CMV/V5 *via* recombination using Gateway LR Clonase (Invitrogen). All coding sequences were confirmed by Sanger sequencing at Genewiz. Adenoviral constructs were packaged into viruses by introducing them into the HEK293A cell line. Adenoviral titers were determined using the Adeno-X qPCR titration kit (Takara Bio USA).

Human H4 neuroglioma cells were plated on a 15 cm culture dish at 4.5 million cells in media consisting of Dulbecco's modified essential medium and 10% (v/v) fetal bovine serum. One day after plating, the cells were cotransduced with adenoviruses encoding Tau (or LacZ for a negative control) and each kinase at a multiplicity of infection of 4 for each virus. After 72 h, the cells were harvested by trypsinization and pelleted, and the pellets were washed with PBS and stored at −80 °C until protein isolation. Total 3xFLAG-Tau (phosphorylated and unphosphorylated) was isolated by incubating the H4 cell lysate with anti-FLAG M2 magnetic agarose beads (Sigma–Aldrich) for 2 h at 4 °C. Beads with bound Tau protein were washed three times with TBST and once with Tris-buffered saline.

The anti-FLAG M2 bead-bound FLAG-Tau from H4 cells was denatured in 8 M urea, reduced, and alkylated using 5 mM Tris(2-carboxyethyl)phosphine and 10 mM chloroacetamide for 45 min at 37 °C. The samples were diluted fivefold with 50 mM TEAB and then digested with Lys-C at a 1:100 (w/w) enzyme-to-protein ratio for 3 h at 37 °C. Trypsin was added to a final enzyme-to-protein ratio of 1:50 (w/w) for overnight digestion at 37 °C. The peptide samples were desalted by SDB-XC (3M Empore). Peptide eluents were vacuum dried. The peptide amounts were measured using the Pierce Quantitative Colorimetric Peptide Assay (Thermo Fisher Scientific). The same amount of peptide was taken from each sample for the subsequent polyMAC phosphopeptide enrichment (Tymora) (25) and phosphopeptide quantification steps. The data of the first replicate were collected using the Q-Exactive HF-X mass spectrometer, and the data of the second replicate were collected using the LTQ-Orbitrap Velos Pro mass spectrometer.

Experimental Design and Statistical Rationale

For the FCMS screening experiments, two independent replicates were conducted in the same manner. Each independent replicate was analyzed by LC–MS with three technical replicates. A protein with valid MS intensities in at least two of three technical replicates was considered a valid identified protein in FCMS. A kinase present in both independent replicates was considered a hit. Albumin was used as a control for Tau to exclude nonspecific interacting kinases. A quantitative comparison of the Tau- and albumin-FCMS samples was performed using a *t* test. For the *in vitro* phosphorylation reactions, two independent reactions were conducted in the same manner. For the analysis of phosphorylated Tau by candidate kinases in H4 cells, two independent replicates were prepared in the same manner. After Lys-C/trypsin digestion, the same amount of peptide was taken from each sample for a quantitative comparison of Tau phosphopeptides between a kinase-Tau sample and the LacZ-Tau control after polyMAC

phosphopeptide enrichment and label-free quantification (LFQ). A quantitative comparison of Tau phosphopeptides between a kinase-Tau sample and the LacZ-Tau control was performed using the *t* test.

RESULTS

FCMS for Tau Kinases

The design of FCMS includes capturing the weakly interacting kinases in a specific IP experiment to overcome the current limitations of identifying unknown kinases and high-throughput mass spectrometric analyses for identification and quantitation (Fig. 1). We take advantage of the self-assembly feature of the Venus fluorescent protein fragments in BiFC, VN155, and VC155, to stabilize these evanescent interactions (21). We started with a publicly available human kinase library, which consists of 559 human kinases and kinase-related protein ORFs (26, 27). Each kinase in the library was fused with the VC155 tag, and the substrate was fused with the VN155 tag. Both the plasmid DNAs encoding the substrate and the kinase library were simultaneously introduced into HEK293T cells. HEK293T cell line was chosen because of its high efficiency of transfection and high protein expression levels. Once a kinase interacted with the substrate in intact cells, the substrate–kinase complex could be stabilized by VN155–VC155 association in the cells. This reconstructed Venus protein from the VN155–VC155 association, not the VN155 or VC155 fragment only, can be specifically isolated using the GFP Nanotrap (28) magnetic agarose beads, and therefore the substrate–kinase complexes can be enriched efficiently. The isolated substrate–kinase complexes were subject to LC–MS/MS for identification and LFQ of the captured kinases.

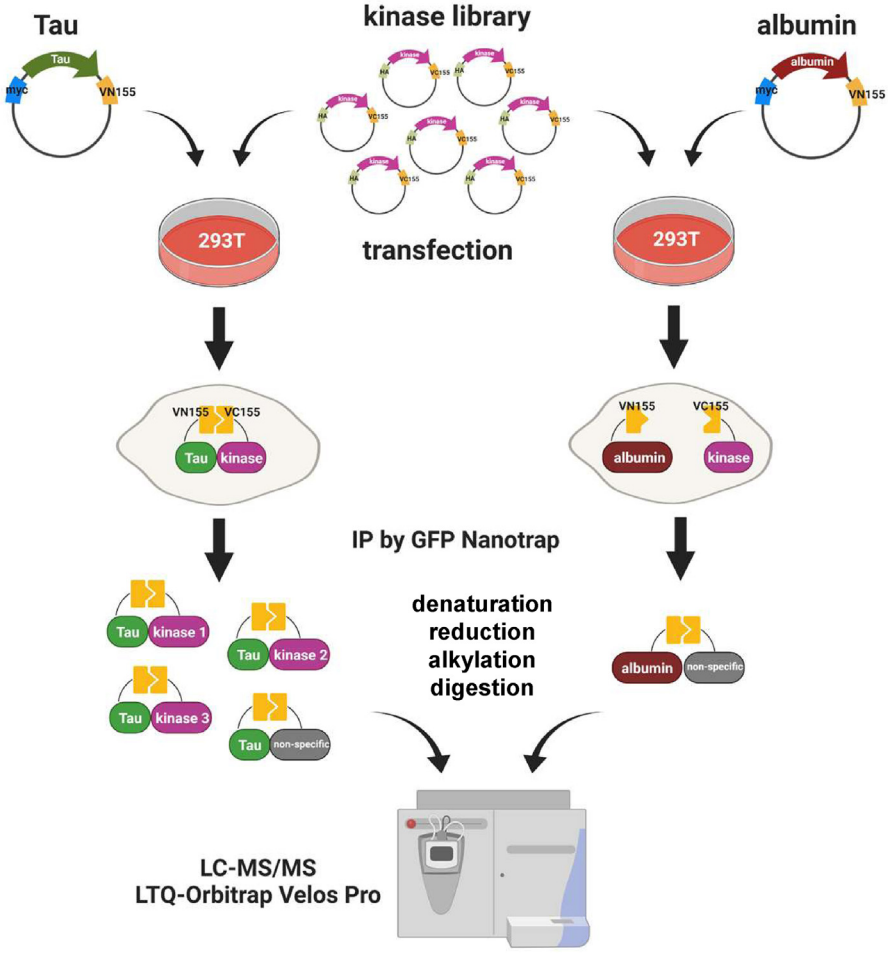

FIG. 1. **Flowchart illustrating the fluorescence complementation mass spectrometry (FCMS) method used for the identification of upstream kinases of Tau.** HEK293T cells were cotransfected with the BiFC vector Myc-VN155 encoding Tau 2N4R (*left*) or the control protein albumin (*right*) and the complementary BiFC vector HA-VC155 encoding a human kinase cDNA expression library encompassing 559 kinases. Cells were lysed, and protein complexes with VN155–VC155 association were immunoprecipitated with GFP Nanobody. Proteins on the beads were reduced, alkylated, and trypsin-digested, and the samples were analyzed by LC–MS/MS for identification and label-free quantitation of kinases. Proteins identified in the albumin control were considered nonspecific interacting proteins. Created with BioRender.com. BiFC, bimolecular fluorescence complementation; cDNA, complementary DNA; HA, hemagglutinin; HEK293T, human embryonic kidney 293T cell line.

One of the major challenges of FCMS is the irreversibility of the BiFC VN–VC self-assembly, which can contribute to problematic false positives from stochastic protein association or nonspecific binding (21). To tackle this problem, in this study, we further increased the specificity by exploring a good negative control. Albumin was chosen to be our negative control for nonspecific binding events in an FCMS screen. Albumin is generated by hepatocytes and then secreted into blood plasma, and thus, it does not typically remain inside a cell. Therefore, we assumed that albumin does not significantly interact with kinases intracellularly. To verify this assumption, we used text-mining tools for protein phosphorylation (eFIP (29, 30), RLIMS-P (31), and iPTMnet (32, 33)) to comprehensively search for any reported kinases of albumin. We found only one identified kinase, the serine/threonine protein kinase FAM20C (34), which is extracellular and not in our human kinase library. In fact, our FCMS results showed that only a small number of kinases were associated with albumin, and most of these kinases were not consistently identified in our replicates. Our FCMS results indicated that most kinases do not specifically associate with albumin, and thus albumin can be used as a good negative control in FCMS. To keep albumin inside the transfected cells, we removed the protein's secretion signal peptide and propeptide (supplemental Fig. S1*A*). Albumin without the secretion signal peptide and the propeptide has a similar size to Tau. Also, the expression level of albumin and Tau was similar in the transfected HEK293T cells (supplemental Fig. S1*B*). These results demonstrated the feasibility of using albumin as a negative control of Tau in the FCMS screening.

In the adult human brain, there are six isoforms of Tau. The N1, N2, and R2 domains of Tau can be alternatively spliced to generate shorter isoforms. Importantly, phosphorylation on N1, N2, and R2 was also identified in AD *postmortem* human brains but not in the control brains (15), indicating possible significance of these sites. Hence, to maximize the scope of kinases to be identified, we chose the longest Tau isoform in the adult human brain, 2N4R, in the FCMS screen.

Identification of the FCMS Tau-Interacting Kinase Proteins

To identify reproducible kinase candidates, we performed two independent biological replicates of FCMS of Tau and selected the kinase hits consistently identified in both biological replicates. Protein quantification is critical for selecting our kinase candidates. To quantify the detected proteins, three MS technical replicates were performed for each sample for LFQ using Proteome Discoverer. To eliminate variation in our samples, the quantification data were normalized by the abundance of vimentin, which is a common nonspecific binding protein of magnetic agarose beads from human cells in IP experiments (35). Indeed, we detected significant protein abundance of vimentin in all MS runs of the FCMS experiments (supplemental data S1, *A* and *B*).

In the first and second biological replicates of FCMS isolation, we identified 759 and 1186 proteins and quantified 334 and 454 proteins, which were statistically different in abundance between the samples of Tau-kinase and albumin-kinase, respectively (Fig. 2*A*). Among these quantified proteins, there were 141 and 162 kinase hits in the first and second biological replicates, respectively. These kinase hits account for a significant portion of each quantified protein set in each biological replicate (42% and 36%, respectively), compared with the ratio of the number of ORFs in the kinase library to the number of human protein-coding genes (~3%). These data highlight the success of kinase isolation *via* BiFC IP. Also, as expected, Tau was the protein with the most significant ratio of protein abundances in comparison of the Tau-kinase sample and albumin-kinase sample. Similarly, albumin was also the protein with the most significant ratio of protein abundances in comparison of the albumin-kinase sample and the Tau-kinase sample.

Notably, in both biological replicates, most of the quantified kinases were Tau-associated kinase hits (137 of 141 and 145 of 162, respectively). Only very few kinase proteins were albumin-associated kinase hits (4 of 141 and 17 of 162, respectively) (Fig. 2*A*). To eliminate randomly associated endogenous kinases from the cells that are not in our human kinase library, we compared the data with our human kinase library (supplemental Fig. S2, *A* and *B*). Most of the kinase protein hits in both biological replicates were included in our human kinase library (135 of 137 [99%] and 144 of 145 [99%], respectively). We also analyzed these albumin-associated kinase hits in the two replicates and observed that most of them were not consistent, and only one kinase hit was consistent in both replicates (supplemental Fig. S2, *C–E*), indicating that albumin has little interaction with most kinases. Also, these albumin-associated kinase hits rarely overlap with Tau-associated kinase hits in the other replicate (supplemental Fig. S2, *F* and *G*). These data demonstrated albumin is a good negative control and overall good specificity of our FCMS method.

To select reproducibly identified and quantified kinase proteins, we overlapped the first and second biological replicates. A total of 101 kinase hits from our human kinase library were consistent in both replicates, accounting for more than 70% kinase hits in both replicates (Fig. 2*B*). These 101 kinase hits were therefore selected as our primary hits because of their consistency in both replicates.

The human kinase library we used consists of 420 protein kinases, 53 kinase-related proteins (regulatory subunits), and 86 nonprotein kinases (carbohydrate, lipid, and nucleotide kinases) (26, 27). As we were primarily interested in identifying new protein kinases of Tau, we manually analyzed the classification of these 101 kinase candidates based on the human kinome data (36, 37). There were 67 protein kinases (supplemental data S2*A*), 6 protein kinase regulatory subunits (supplemental data S2*B*), and 28 nonprotein kinases

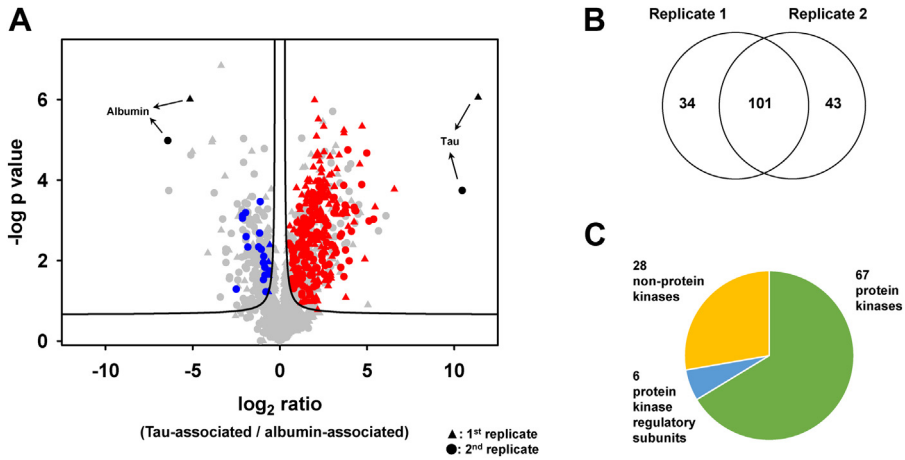

FIG. 2. **FCMS identification of Tau kinase hits.** *A,* volcano plot from two biological replicates of our FCMS analysis showing the proteins quantified in the co-IP of Tau and the kinase library. Statistical significance was assessed through a permutation-based FDR *t* test (FDR = 0.05; S0 = 0.2), based on three LC–MS technical replicates. Tau- and albumin-associated kinase hits are represented by *red* and *blue symbols*, respectively. Data from the first and second biological replicates are shown as *triangles* and *circles*, respectively. *B*, Venn diagram showing the overlap of the library-verified Tau-associated kinase hits between the two FCMS replicates. *C*, Pie chart showing library-verified Tau-associated protein kinases, protein kinase regulatory subunits, and nonprotein kinases reproducible in both replicates. co-IP, coimmunoprecipitation; FCMS, fluorescence complementation mass spectrometry; FDR, false discovery rate.

(supplemental data S2C). The protein kinases and associated related regulatory subunits accounted for 72% of all identified kinase hits (Fig. 2*C*). These 67 protein kinases were therefore selected as our primary hits because of their consistency in both replicates.

Analyses of the Novel FCMS Kinase Hits

Protein expression profiles can be significantly distinct in different tissues or organs. Kinases must be expressed in the human brain to phosphorylate Tau. To validate the expression of these kinases in the human brain, we compared our 67 protein kinase hits with the RNA-Seq data of the human brain cerebral cortex downloaded from the Human Protein Atlas (HPA) database (38, 39). The RNA-Seq data in the HPA database were displayed as transcripts per million reads, which is a normalization method for the comparison of gene expression between different tissues or organs. We considered all genes with transcripts per million >0 in the HPA cerebral cortex data (18,138 genes). We found that all our 67 kinases were detected in the human cerebral cortex based on the HPA data (Fig. 3*A*), showing high confidence for our protein kinase hits.

Next, to further validate the presence of these kinases in real tauopathy patients, we compared the 67 kinase hits with recently published clinical proteomic data. Since AD is the most predominant tauopathy disease, we used AD proteomic data for this validation. We chose the clinical proteomic data reported by Bai *et al.* (40) (14,513 proteins and 12,018 genes). Most of our kinase hits (59 kinase hits) were found in this AD postmortem human brain proteome (Fig. 3*B*). Furthermore, since the phosphorylation is a critical regulation of kinase activities, we also compared our data with the AD phosphoproteome in the same study. Indeed, the phosphopeptides of a majority of our kinase hits were detected in the phosphoproteomic data of Bai *et al.* (46 of 59, 78%) (Fig. 3*C*), and some known kinases of Tau (*e.g.*, ABL2, BRSK2, and mitogen-activated protein kinase 1 (MAPK1)/ERK2) showed higher phosphorylation levels in their AD postmortem frontal gyrus samples compared with their nondisease control samples. Moreover, hyperphosphorylation of Tau was also observed in the phosphoproteomic data of Bai *et al.*, suggesting that the activities of these kinases in the AD cohort were high. Also, another phosphoproteome of human AD postmortem brains recently reported by Morshed *et al.* (41) showed aberrant phosphorylation of kinases and Tau, further suggesting that the phosphorylation of these kinases was significantly associated with AD pathological markers. Therefore, to further validate our 59 FCMS protein kinase hits, we compared our data with this phosphoproteome. In fact, many of our FCMS protein kinase hits also overlap with the AD phosphoproteomic data, including known Tau kinases (*e.g.*, BRSK1, CSNK1E, SRC, etc.) and our novel kinase candidates (*e.g.*, MAST1, LMTK2, etc.) (Fig. 3*D*). Taken together, the consistency between our data and the published data strongly supported the kinase hits in our FCMS of Tau. Therefore, we chose the 59 kinase hits that were also found in the proteomic data of Bai *et al.* for the subsequent analyses.

Our kinase library includes many known kinases of Tau, so we expected to capture at least a subset of these using our FCMS approach. By using text-mining tools (eFIP (29, 30), RLIMS-P (31), and iPTMnet (32, 33)) and manually searching in the literature, we found that 23 kinases are known kinases of Tau, and 36 kinases have not yet been reported to be Tau kinases (supplemental data S2*A*, Fig. 3, *E* and *F*). We detected

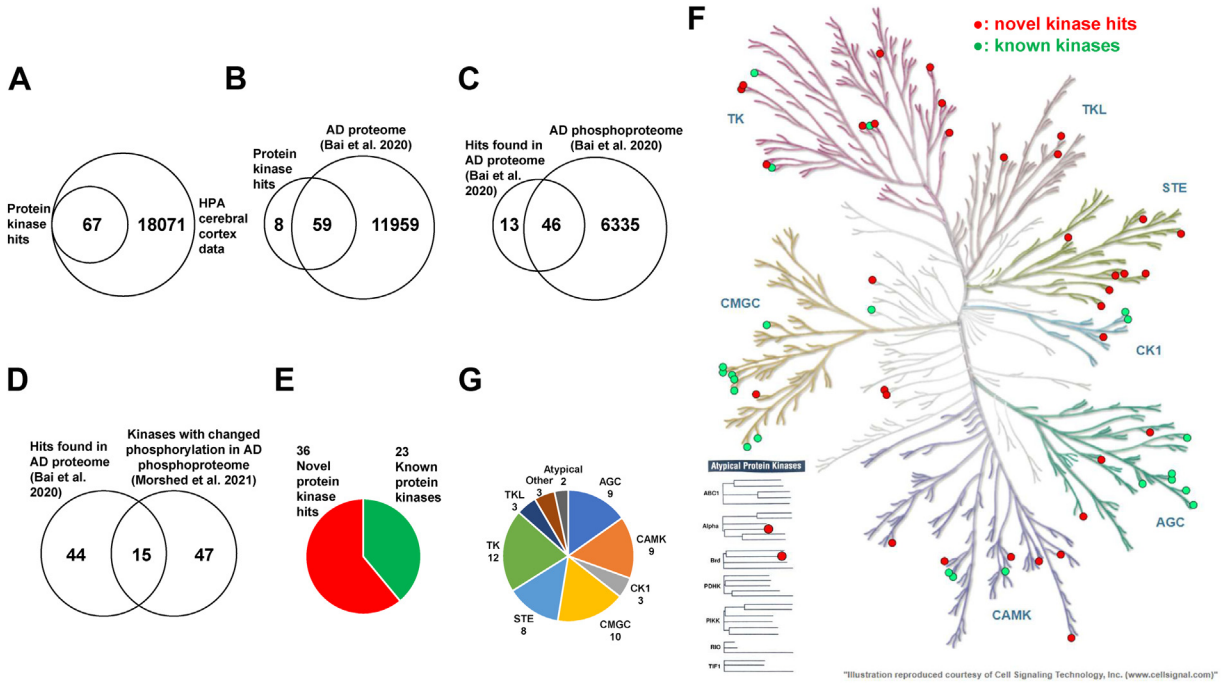

FIG. 3. **Analyses of the FCMS kinase hits of Tau.** Venn diagram showing the overlap between the Tau-associated kinase hits and the human brain cerebral cortex data in the Human Protein Atlas (HPA) (*A*), the AD proteome dataset reported by Bai *et al.* (*B*), the AD phosphoproteome dataset reported by Bai *et al.* (*C*), and the kinases with changed phosphorylation in the AD phosphoproteome reported by Morshed *et al.* (*D*). Pie chart showing the distribution of Tau-associated kinase hits from our FCMS analysis between known and novel protein kinases (*E*). *F*, kinome map visualization of kinase hits from our FCMS analysis. Nodes are colored *red* and *green* for novel and known kinases, respectively (*F*). The classification of the 59 kinase hits (*G*). AD, Alzheimer's disease; FCMS, fluorescence complementation mass spectrometry.

many well-characterized kinases of Tau, including GSK3A, SRC, ABL2, and so on. The identification of many known kinases of Tau validated the effectiveness of our FCMS and therefore further strengthened the reliability of these 36 novel candidate kinases. These 36 kinases thus constituted our final list of novel kinase candidates identified *via* FCMS screening (supplemental data S2*A*). In addition, Tau was reported to be phosphorylated by a wide variety of protein kinases. The currently known protein kinases of Tau belong to at least 7 of the 10 classes of human protein kinases (4, 5, 12–14, 36, 37). Our 59 kinase hits cover most of the classes of human protein kinases (9 of 10, except for the receptor guanylate cyclases group) (supplemental data S2*A*, Fig. 3, *F* and *G*), suggesting an unbiased feature of the FCMS hits.

Kinases can interact with many proteins, including kinases themselves, to generate intricate protein–protein interaction networks (42). In an FCMS screening, kinases may synergistically or indirectly associate with the substrate of interest with other direct interactors of the substrate. Therefore, we analyzed the physical protein interaction networks of our 101 kinase hits using STRING (43) (supplemental Fig. S3). Among all our FCMS kinase hits, 72 of these are apparently involved in complex physical interaction networks. Several interacting clusters could be identified, including clusters of cyclin-dependent kinases (CDK1, CDK2, and CDK4), PKC (AKT1 and PKC isoforms PRKCA, PRKCB, and PRKCZ), cAMP-dependent protein kinase (PRKAR1A, PRKAR2A, PRKAR2B, PRKAG1, and PRKAA2), and kinases in the MAPK pathway (MAPK1, MAPK3, MAPK12, MAPK13, MAPK14, MAP2K2, MAP2K6, MAPKAPK3, and MAPKAPK5). These kinases and kinase-related regulatory subunits in the same clusters tend to physically associate together so that they are more likely to be captured by FCMS concurrently. These functionally related kinases may all be responsible for the phosphorylation of Tau. For example, all the PKC isoforms and AKT1 in our FCMS hits are known kinases of Tau. On the other hand, there were 25 kinases that did not show involvement in any physical interactions in the STRING analyses. These kinases are more likely to directly and independently interact with Tau, or they may interact with Tau *via* other mediators that are not included in the database or are still unknown yet. In summary, the STRING analyses can provide more supporting evidence for our FCMS kinase hits.

Interestingly, we also captured 28 nonprotein kinases, including the lipid kinase SPHK2, the nucleoside diphosphate kinase DTYMK, and the hexokinases (HKs) HK2 and HK3, and so on. Some of the nonprotein kinase hits (CKMT1A, PFKP, and AK1) were identified in a previously reported interactome of phosphorylated Tau (44). Since Tau can interact with nucleotides (45–48), lipid bilayers (49–51), and other protein

kinases (supplemental Fig. S3), these nonprotein kinases may be captured because of indirect interactions with Tau.

In vitro *Phosphorylation Assays and pIMAGO Phosphorylation Detection*

FCMS is capable of capturing kinases that can physically associate with a bait substrate protein. To confirm that these kinase candidates are able to phosphorylate Tau, we performed *in vitro* phosphorylation assays using purified recombinant Tau and kinases.

Among our 36 kinase candidates, there were several candidates (MAP2K2, MAP2K6, MAP4K2, and MAPKAPK5) belonging to the MAPK pathway. Since many kinases in the MAPK pathway are well-characterized Tau kinases (4, 5, 12–14), we excluded these candidates from our validation. Also, we did not test CDK4 since the cyclin necessary for its activity in our *in vitro* phosphorylation assays is unknown. We expressed and purified HA-tagged kinases candidates from HEK293T cells using anti-HA antibody beads. The human HEK293T cells can provide the correct protein folding and essential post-translational modifications, which are critical for the activities of many kinases. On the other hand, we expressed and purified His-tagged Tau from *E. coli* using nickel–nitrilotriacetic acid beads based on a previous report (52). Previous studies have shown that recombinant Tau prepared using an *E. coli* expression system is nonphosphorylated (53, 54). After optimizing the expression and purification methods for Tau and kinase, we successfully obtained purified Tau, 15 candidate kinases, and one known Tau kinase GSK3A (supplemental Fig. S4*A*). To simplify the subsequent analyses, the kinase assays were performed using on-bead kinases for the convenience of removing kinases after the reactions were complete. To ensure that there was no Tau phosphorylation resulting from nonspecific binding of endogenous kinases in the cell lysate, we used anti-HA antibody beads treated with a lysate prepared from cells without ectopic kinase expression as a negative control.

Tau phosphorylation was monitored by pIMAGO (phosphoimaging), a nanopolymer and nonantibody reagent for phosphorylation detection. The method is based on water-soluble and globular nanopolymers (*i.e.*, dendrimers) with modifications of titanium for capturing phosphate groups and biotin for detection by avidin-Fluor (55–58). This reagent can substitute for phospho-specific antibodies in a Western blotting analysis without the need of site-specific antibodies. The pIMAGO method can also replace conventional kinase assays using radiolabeled ATP to avoid safety issues. We optimized *in vitro* kinase reactions for different protein kinases by tuning various parameters (59). Limited by *in vitro* kinase reaction conditions such as buffer, pH, divalent ions Mg^{2+} and Mn^{2+}, ATP concentrations, reaction time, cofactors, and so on, we successfully observed that four of our FCMS candidate kinases, OXSR1, DAPK2, CSK, and ZAP70, could phosphorylate Tau *in vitro* (Fig. 4*A*). Notably, OXSR1 and DAPK2 are not involved in the interaction networks of our kinase hits revealed by our STRING analysis (supplemental Fig. S3), suggesting that they could potentially interact with Tau directly instead of indirectly *via* other interactors.

Time-Course Tau Phosphorylation Reveals Specific Phosphorylation Sites by the Kinase Candidates

Tau is a complex phosphoprotein with 85 phosphorylation sites in the longest isoform expressed in the adult human brain (2N4R) (4, 12–14). In AD brains, some phosphorylation events were commonly observed, whereas others were less commonly detected (15), suggesting that certain phosphorylated sites may be more dominant in AD pathogenesis. To investigate whether our four Tau kinase candidates could phosphorylate pathologically relevant sites of Tau specifically, we performed an *in vitro* time-course phosphorylation reaction coupled with LC–MS analysis using the purified recombinant kinases and Tau protein. The *in vitro* phosphorylation time-course reactions were again conducted using on-bead kinases, and beads treated with a lysate prepared from cells without ectopic kinase expression were used as a negative control. In a reaction, the substrate Tau was much more than the kinase (the molar ratio of substrate to kinase >10) to avoid deletion of the substrate over the reaction course so that we could investigate whether we can observe a persistent increase of phosphorylation by performing time-course experiments and collecting reaction samples at 0, 1.5, and 3 h. To compare the relative intensities of phosphorylation between kinase-treated and kinase-null samples at different time points, we labeled our time-course phosphorylation samples with isobaric TMTs for multiplexed quantification (Fig. 4*B*). Our LC–MS detection method achieved a total sequence coverage of ≥69% for the Tau 2N4R isoform (supplemental Fig. S4*B*). We normalized the TMT intensities of each peptide based on the total intensity of unphosphorylated Tau peptides, which was assumed to remain constant during the reaction course.

We successfully detected multiple Tau phosphorylation events that reproducibly increased in the kinase-present samples temporally but not in the kinase-null samples (Figs. 4, *C–H*, S4, *C–G*, supplemental datas S3 and S4). We observed a reproducible increase of phosphorylation at S199, a residue known to be phosphorylated by GSK3A, in a sample of GSK3A-treated Tau (Figs. 4*H* and S4*G*), validating our *in vitro* kinase assay design. In a sample of DAPK2-treated Tau, we detected a reproducible increase of phosphorylation at Tau S214 (Figs. 4*D* and S4*C*). In the OXSR1-treated Tau, we detected a reproducible increase of phosphorylation at Tau S324 and T30 (Figs. 4E and S4*D*). In a sample of ZAP70-treated Tau, we detected reproducible increases of phosphorylation at Tau Y29 and Y197 (Figs. 4*F* and S4*E*). In a sample of CSK-treated Tau, we detected a reproducible increase of phosphorylation of Tau Y29 (Figs. 4*G* and S4*F*). These results indicated that DAPK2 could potentially phosphorylate Tau at S214, OXSR1 could phosphorylate Tau at

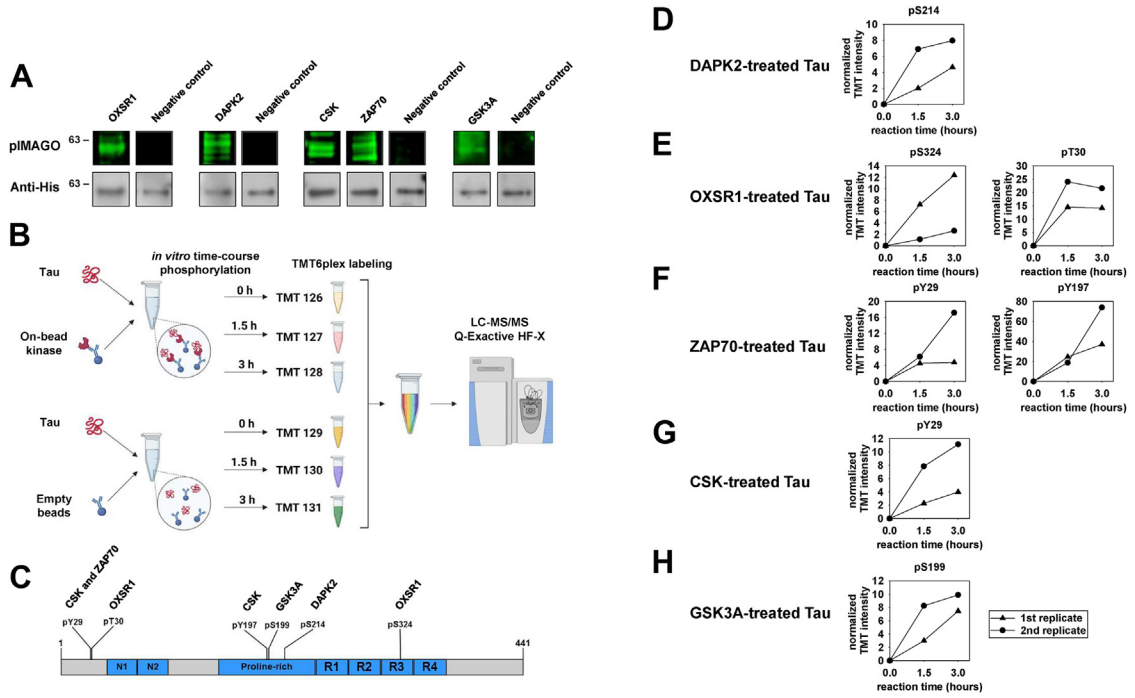

FIG. 4. **Validation of the FCMS kinase hits of Tau.** *A*, the pIMAGO results of *in vitro* phosphorylation. Anti-His immunoblotting was used as the loading control for His-tagged Tau. A known kinase of Tau, GSK3A, was used as a positive control for the *in vitro* phosphorylation. *B*, experimental workflow for *in vitro* time-course phosphorylation reaction, TMT6plex labeling, and LC–MS/MS. Created with BioRender.com. *C*, an overview of detected phosphorylated sites of the TMT6plex-labeled kinase-treated 2N4R Tau measured in the LC–MS/MS. *D–H*, *in vitro* time-course phosphorylation of Tau using DAPK2 (*D*), OXSR1 (*E*), ZAP70 (*F*), CSK (*G*), and GSK3A (*H*). Data are shown as the average normalized TMT intensities of all detected phosphorylated peptides with different modifications (*e.g.*, methionine oxidation) or trypsin miscleavage. Normalization was performed based on the intensities at time = 0 in the kinase-present sample (TMT 126), and then the background intensities were subtracted. FCMS, fluorescence complementation mass spectrometry; pIMAGO, phosphorylation imaging; TMT, tandem mass tag.

S324 and T30, ZAP70 could phosphorylate Tau at Y29 and Y197, and CSK could phosphorylate Tau at Y29. Taken together, these results demonstrated that DAPK2, OXSR1, CSK, and ZAP70 are promising Tau kinase candidates identified using our FCMS approach for future exploration.

The Kinase Candidates can Increase Phosphorylation of Tau in the H4 Neuroglioma Cells

To explore whether the kinase candidates could induce Tau phosphorylation in living human cells, we coexpressed Tau and the kinases in the human H4 neuroglioma cell line, a commonly used cell line in AD research (supplemental Fig. S5*A*) (60–64). The cells were cotransduced with adenoviruses encoding 3xFLAG-tagged Tau and the HA-tagged kinase candidates (or the control protein LacZ), and lysates prepared after a 72 h incubation period were analyzed *via* Western blotting. We found that all four kinases were expressed along with Tau, and the Tau expression levels were similar across all samples (supplemental Fig. S5*B*). Next, Tau was isolated from lysates of H4 cells coexpressing the protein with a kinase candidate or LacZ using anti-FLAG beads, and the immunoprecipitated protein was analyzed *via* LC–MS to assess differences in the phosphorylation profiles of Tau proteins isolated from cells with or without ectopic kinase expression. The phosphopeptides were enriched by polyMAC (25) before LC–MS runs.

All four candidate kinases were found to induce a significant increase in Tau phosphorylation in H4 cells (Fig. 5 and supplemental data S5). Many of the annotated Tau phosphorylation sites identified here are pathologically relevant and occur in both the early and late stages of AD. For example, Tau has been shown to be phosphorylated at T181, S199, and S202 in early stage AD and at T175, S198, and S205 during later stages of the disease (15). While we did not find the Tau phosphorylation that we detected in our *in vitro* time-course phosphorylation, we observed increased phosphorylation at these disease-associated phosphosites, underlining their significance in AD. Notably, multiple phosphorylation sites were unexpectedly elevated in H4 cells with coexpression of Tau and a kinase candidate, especially in the H4 cells expressing the CSK or ZAP70 tyrosine kinase, which showed the evidence of Tau phosphorylation at several serine and threonine residues. While the sample preparation including phosphopeptide enrichment might have introduced biases in the experiment, it has been reported that tyrosine kinases can activate downstream serine–threonine kinases to increase the serine and threonine phosphorylation of Tau. For example, the tyrosine kinase FYN can activate the serine–threonine kinases

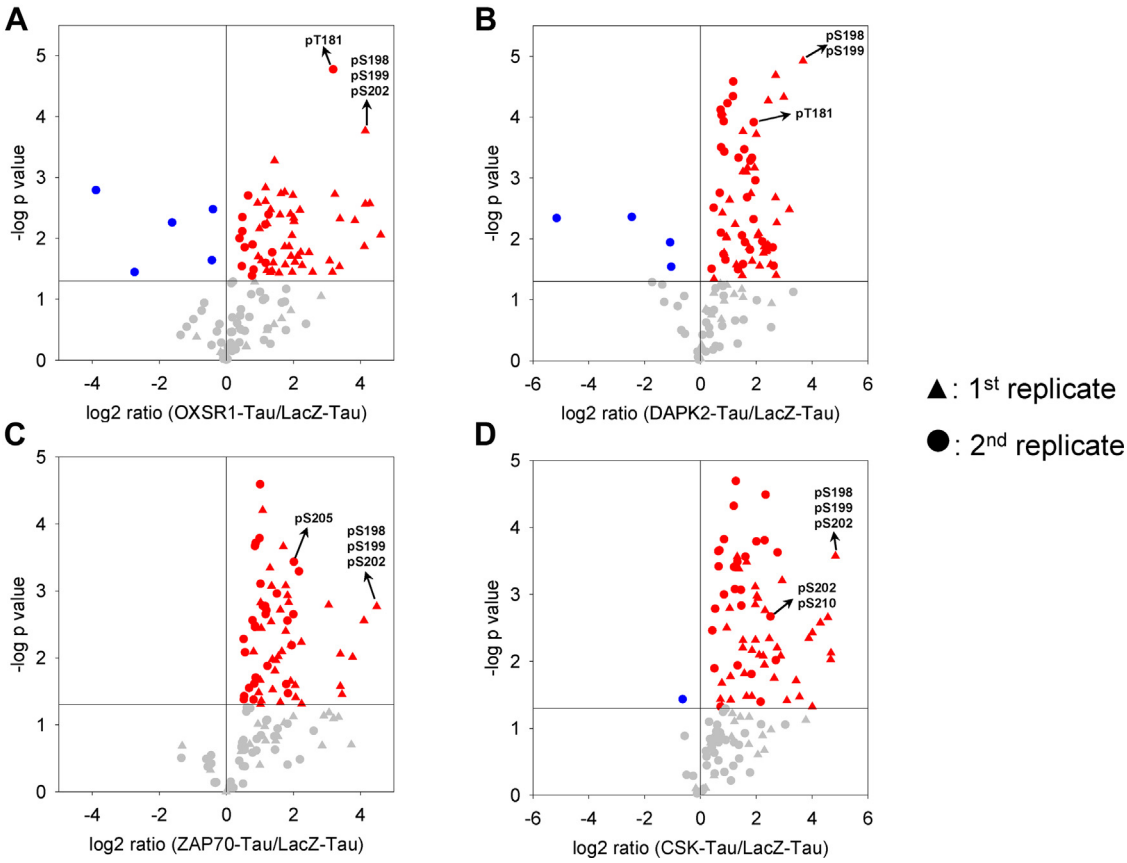

FIG. 5. **Comparison of Tau phosphopeptides between kinase-Tau and LacZ-Tau overexpression H4 cells.** *A*, OXSR1-Tau *versus* LacZ-Tau. *B*, DAPK2-Tau *versus* LacZ-Tau. *C*, ZAP70-Tau *versus* LacZ-Tau. *D*, CSK-Tau *versus* LacZ-Tau. The volcano plots show differences of label-free quantified Tau phosphopeptides between the kinase- and lacZ-expressing H4 cells. Phosphopeptides were enriched using polyMAC. Phosphopeptides that were more abundant in kinase-expressing cells are represented by *red symbols*. Phosphopeptides that were more abundant in kinase-null cells are represented by *blue symbols*. Data from the first and second replicates are shown with *triangular* and *circular symbols*, respectively.

GSK3B and MEK (12). In our STRING analyses, we observed that CSK and ZAP70 are both involved in complex interaction networks with many serine–threonine kinases (supplemental Fig. S3), suggesting that these two tyrosine kinases could activate downstream serine–threonine kinases. These results further highlight the importance of these kinase candidates for Tau phosphorylation in human cells, in turn suggesting that the kinases could play a role in the pathogenesis of AD and other tauopathies. Although we did not observe annotated tyrosine phosphorylation of Tau in CSK- or ZAP70-expressing H4 cells, we detected increased levels of Tau phosphopeptide containing Y197 (supplemental data S5), implying possible phosphorylation of this residue. Taken together, these results suggested that the four kinase candidates can contribute to Tau hyperphosphorylation in human neuroglioma cells.

DISCUSSION

The phosphorylation of Tau is a significant pathological phenomenon in AD and other tauopathies that plays a pivotal role in the protein's dissociation from microtubules and subsequent aggregation, leading to NFT formation (4, 5). Although the importance of Tau kinases in AD and other tauopathies has been acknowledged, the lack of systematic approaches to reveal unknown Tau kinases remains a major obstacle. Additional knowledge about Tau kinases could potentially stimulate the development of therapeutic strategies for tauopathy diseases. Despite the fact that some attempts have been made to uncover new kinases of Tau, those endeavors were limited by the nature of the approaches, including a loss of information because of weak interactions in co-IP or the fact that an incomplete kinase library was used. Using the FCMS strategy and a more comprehensive human kinase library with 559 kinases and kinase-related proteins, we uncovered 36 unreported kinase candidates of Tau. Using *in vitro* phosphorylation reactions followed by pIMAGO or time-course LC–MS analyses, we revealed that four of these kinases, OXSR1, DAPK2, ZAP70, and CSK, could phosphorylate Tau *in vitro*.

OXSR1 was originally identified as having 39% sequence homology to the oxidative stress–related kinase SOK1 (Ste20/

oxidant stress response kinase-1). Therefore, it was proposed to be involved in the oxidative stress response and named OXSR1 (65). Subsequent investigations indicated that it is actually activated by osmotic stress instead of oxidative stress (66). Some evidence has suggested that hyperosmotic stress is a potential pathogenic factor of AD (67, 68), and OXSR1 was reported to be upregulated in AD patients (69). In the *in vitro* phosphorylation time course, we observed that OXSR1 could potentially phosphorylate Tau on S324 and T30. The phosphorylation of S324 was recently detected in AD patients (44) and can result in reduced Tau affinity for microtubules (70), indicating the potential importance of OXSR1 in AD. Many kinases responsible for S324 phosphorylation have been reported (4, 5, 12–14). The phosphorylation of T30 was also recently reported in AD patients (15). However, there are only a few identified kinases responsible for T30 phosphorylation, including LRRK2, PSK1/2, and TTBK1/2 (4, 5, 12–14). Furthermore, the phosphorylation extent of the sequence region containing T30 (from D25 to K44 of Tau 2N4R) was higher in AD patient cohorts (15), and there are only a few possible phosphosites (Y29, T30, and T39) in this region. Hence, the observation of phosphorylated T30 in AD patients indicates that this phosphosite may be important in AD. However, the roles of phosphorylated T30 in AD or other tauopathies remain largely unknown. Notably, we observed that the phosphorylation of T30 did not increase after 1.5 h of reaction time. This suggests that T30 might be a less specific phosphosite of OXSR1, or that some other factors could affect the phosphorylation of T30 by OXSR1. In a previous study, it was shown that prephosphorylation of some Tau phosphosites can have an inhibitory effect on the phosphorylation of other Tau phosphosites (71). The phosphorylation of (an)other phosphosite(s) by OXSR1, probably S324, might inhibit the phosphorylation of T30 in the later stage of the *in vitro* phosphorylation.

DAPK2 belongs to the death-associated protein kinase (DAPK) family, which is a strong tumor suppressor and a newly identified regulator of mammalian target of rapamycin, apoptosis, and autophagy signaling pathways (72). These signaling pathways have been suggested to be AD related (73–75). Its homolog, DAPK1, can interact with Tau and increase the phosphorylation of Tau in transfected HEK293 cells (76), suggesting its potential to be a kinase of Tau. In the *in vitro* time-course phosphorylation, we observed that DAPK2 is capable of phosphorylating S214. Phosphorylated S214, one of the most common AD-related phosphosites (7, 15, 77, 78), can decrease the binding affinity between Tau and microtubules (79). Many well-characterized Tau kinases can phosphorylate this site (4, 5, 12–14). In a recent report by Wesseling *et al.* (15), phosphorylated S214 was detected in around 60% of their studied AD cohort. Therefore, our data suggest that DAPK2 is potentially an important candidate kinase for Tau.

ZAP70 is a homolog of the known Tau kinase SYK (80), suggesting that it too could be a *bona fide* Tau kinase. SYK is a kinase of Tau and an activator of another Tau kinase, GSK3B (81–83). ZAP70 is a well-characterized tyrosine kinase involved in signal transduction in T cells, but it is also expressed in neurons (38, 39). In fact, the expression level of ZAP70 was higher in AD hippocampus (84). Also, AD risk factors apolipoprotein E and TREM2 can activate ZAP70 to trigger downstream signaling pathways (85, 86). These observations indicate that ZAP70 is a potentially critical kinase in AD pathogenesis.

CSK regulates the activities of Src family protein kinases (87). It was found in NFTs (88), suggesting its potential involvement in producing hyperphosphorylated Tau. Also, CSK was reported to be upregulated in AD patients (69). Notably, our data showed that both ZAP70 and CSK can phosphorylate Y29 *in vitro*; however, there have not yet been any reported kinases of Tau Y29 (4, 12–14), indicating the novelty of these results. In addition, like the phosphorylation of T30, the phosphorylation of Tau on Y29 was also recently reported in AD patients in a sequence region with a higher extent of phosphorylation in the AD cohort (10), suggesting that Y29 phosphorylation mediated by ZAP70 or CSK could play a key role in AD pathogenesis.

Using STRING analysis, we observed that our kinase hits can form complex physical interaction networks, including several clusters (supplemental Fig. S3). Some clusters are enriched with kinase groups, such as CDKs, tyrosine kinases, casein kinases, MAPKs, and so on. Notably, there are also several kinase hits that do not form physical protein interaction networks with other kinase hits. It is more likely that these kinases are less relevant to other known kinases of Tau and can directly recognize Tau. In fact, two of our validated kinase candidates, DAPK2 and OXSR1, do not show involvement in the STRING networks.

There were also some other potential kinase candidates in our FCMS hits. For example, BRD3 is a member of the bromodomain and extraterminal domain (BET) family (89), which can specifically bind to acetylated histones for regulating gene transcription. The BET proteins have kinase activities to phosphorylate RNA polymerase II for transcription regulation. Abnormal expression of BET proteins has been linked to cancer, and small-molecule inhibitors targeting the BET proteins, such as JQ1, have been developed (90). Interestingly, some recent reports show that JQ1 can alleviate the disease end points of AD mouse models (91, 92). One study even shows that Tau phosphorylation at Ser369 can be reduced by JQ1 treatment (91). Although we did not successfully detect phosphorylation of BRD3-treated Tau in our *in vitro* phosphorylation assays, this evidence from the literature supports our FCMS data that BRD3 may be a potential novel kinase of Tau or a kinase that can activate downstream Tau kinases. Moreover, CDK4 is a CDK that is clinically significant in cancers such as melanoma and breast cancer. Interestingly, dysregulated gene expression of CDK4 was reported in AD patients (93), and CDK4 inhibitors were reported to protect

neurons from cell death because of nerve growth factor deprivation and beta-amyloid (Aβ) toxicity (94). Aβ can activate many downstream kinases that in turn induce the hyperphosphorylation of Tau (12). Based on the evidence in the literature and our FCMS data, we hypothesize that CDK4 may be a Tau kinase induced by Aβ signaling. Validation of our novel FCMS kinase hits including BRD3 and CDK4 will be a goal of future studies.

Also, genetic knockout or knockdown studies in animal models will be a further validation aiming for the biological importance of these kinases *in vivo*. The roles of several Tau kinases have been investigated in Drosophila and mice, and these studies successfully demonstrated their significance in Tau protein aggregation, synaptic dysfunction, and neurotoxicity (81, 95–97). The confirmation of these Tau kinases and in particular their roles in Tau pathogenicity will provide valuable information for developing kinase inhibitor drugs to alleviate neurodegeneration caused by abnormal Tau phosphorylation.

In our FCMS screening, we also identified many nonprotein kinases in our FCMS screening. In any IP experiments, indirectly associated protein can also be isolated. In fact, many nonprotein kinase hits can interact with known protein kinases of Tau (supplemental Fig. S3). For example, the hexokinases HK2 and HK3 can associate with AKT1, and SPHK2 can associate with PRKCE and SRC *via* TYK2. Also, SPHK2 is responsible for the phosphorylation of sphingosine to form sphingosine-1-phosphate, which is located in lipid bilayers (98), with which Tau has been reported to interact (49–51); therefore, the Tau protein in our FCMS may indirectly associate with lipid kinases like SPHK2 *via* binding to lipid bilayers. The nucleoside diphosphate kinase DTYMK is an RNA-binding protein (99). Given that Tau can also interact with DNA (47, 48) and RNA (45, 46), Tau may have an indirect association with nucleoside diphosphate kinases such as DTYMK. These pieces of evidence could explain why these nonprotein kinases were captured using our FCMS approach. In fact, the nonprotein kinase hits CKMT1A, PFKP, and AK1 were all identified in a previously reported interactome of phosphorylated Tau (44).

There are some limitations of using our FCMS to uncover novel kinases of Tau. The kinase constructs we used in this study might not fairly represent the comprehensive kinase proteoforms, including isoforms and other sequence variations, expressed in AD human brains. Similarly, we used only the 2N4R isoform of Tau. Thus, we may miss kinases that preferentially interact with specific Tau isoforms. Moreover, the HA tag and VC tag may affect the structures, post-translational modifications, and catalytic activities of the kinases. Likewise, the Myc and VN tags of Tau may interfere with the interaction between Tau and some of its kinases. Also, the kinase library we used here consists of 420 protein kinases (26, 27), which does not encompass all the 538 known human protein kinases (36, 37).

Here, we have demonstrated the application of FCMS for screening upstream kinases of Tau and validated the ability of the kinase candidates to phosphorylate Tau. Numerous known kinases and novel kinase hits of Tau were identified. Four kinases in our FCMS hits successfully displayed the capability of phosphorylating Tau *in vitro*. These results indicate the plausibility of these four kinase candidates to be *bona fide* Tau kinases. Our identification of promising kinase candidates not only supports the hypothesis that Tau can be phosphorylated by unknown kinases to become pathogenic but also provides a more comprehensive kinase repertoire to facilitate the development of Tau phosphorylation inhibitors as potential drugs for AD in the future.

DATA AVAILABILITY

The MS proteomics data have been deposited to the ProteomeXchange Consortium (100) *via* the jPOST partner repository (101) with the dataset identifier PXD036956 for ProteomeXchange.

Supplemental data—This article contains supplemental data.

Acknowledgments—We thank Thermo Fisher Scientific's generous support for the use of Q-Exactive HF-X mass spectrometer.

Funding and additional information—This project has been funded by the National Institutes of Health grants 3RF1AG064250 (to W. A. T.) and R03NS108229 (to J. C. R.). The content is solely the responsibility of the authors and does not necessarily represent the official views of the National Institutes of Health.

Author contributions—D.-S. K., Y. D., A. G. D., S. M., M. C. H., J.-C. R., and W. A. T. conceptualization; D.-S. K., Y. D., A. G. D., S. M., M. C. H., J.-C. R., and W. A. T. methodology; D.-S. K. validation; D.-S. K., A. G. D., S. M., M. C. H., J.-C. R., and W. A. T. formal analysis; D.-S. K., Y. D., A. G. D., and S. M. investigation; J.-C. R., and W. A. T. resources; D.-S. K. data curation; D.-S. K. and W. A. T. writing–original draft; D.-S. K., S. M., J.-C. R., and W. A. T. writing–review & editing; W. A. T. supervision; W. A. T. project administration; J.-C. R. and W. A. T. funding acquisition.

Conflict of interest—The authors declare no competing interests.

Abbreviations—The abbreviations used are: Aβ, beta-amyloid; AD, Alzheimer's disease; BET, bromodomain and extraterminal domain; BiFC, bimolecular fluorescence complementation; CDK, cyclin-dependent kinase; cDNA, complementary DNA; co-IP, coimmunoprecipitation; FCMS, fluorescence complementation mass spectrometry; FDR, false discovery rate; HA, hemagglutinin; HEK, human embryonic kidney cell line; HK, hexokinase; HPA, Human Protein Atlas;

IP, immunoprecipitation; LFQ, label-free quantification; MAPK, mitogen-activated protein kinase; MS, mass spectrometry; NFT, neurofibrillary tangle; pIMAGO, phosphorylation imaging; TBST, Tris-buffered saline supplemented with 0.1% Tween-20; TEAB, triethylammonium bicarbonate; TMT, tandem mass tag.

Received July 24, 2022, and in revised form, November 9, 2022
Published, MCPRO Papers in Press, November 13, 2022, https://doi.org/10.1016/j.mcpro.2022.100441

REFERENCES

1. 2022 Alzheimer's disease facts and figures. *Alzheimers Demen.* **18**, (2022), 700–789
2. 2021 Alzheimer's disease facts and figures. *Alzheimer's Demen.* **17**, (2021), 327–406
3. Knopman, D. S., Amieva, H., Petersen, R. C., Chételat, G., Holtzman, D. M., Hyman, B. T., *et al*. (2021) Alzheimer disease. *Nat. Rev. Dis. Primers* **7**, 33
4. Arendt, T., Stieler, J. T., and Holzer, M. (2016) Tau and tauopathies. *Brain Res. Bull.* **126**, 238–292
5. Guo, T., Noble, W., and Hanger, D. P. (2017) Roles of tau protein in health and disease. *Acta Neuropathol.* **133**, 665–704
6. Cho, J. H., and Johnson, G. V. W. (2003) Glycogen synthase kinase 3β phosphorylates tau at both primed and unprimed sites: differential impact on microtubule binding. *J. Biol. Chem.* **278**, 187–193
7. Zhu, B., Zhang, L., Creighton, J., Alexeyev, M., Strada, S. J., and Stevens, T. (2010) Protein kinase A phosphorylation of tau-serine 214 reorganizes microtubules and disrupts the endothelial cell barrier. *Am. J. Physiol. - Lung Cell Mol. Physiol.* **299**, 493–501
8. Despres, C., Byrne, C., Qi, H., Cantrelle, F. X., Huvent, I., Chambraud, B., *et al*. (2017) Identification of the Tau phosphorylation pattern that drives its aggregation. *Proc. Natl. Acad. Sci. U. S. A.* **114**, 9080–9085
9. Zhang, X., Hernandez, I., Rei, D., Mair, W., Laha, J. K., Cornwell, M. E., *et al*. (2013) Diaminothiazoles modify Tau phosphorylation and improve the tauopathy in mouse models. *J. Biol. Chem.* **288**, 22042–22056
10. Lee, J. S., Lee, Y., Andre, E. A., Lee, K. J., Nguyen, T., Feng, Y., *et al*. (2019) Inhibition of Polo-like kinase 2 ameliorates pathogenesis in Alzheimer's disease model mice. *PLoS One* **14**, e0219691
11. Wang, Y., and Mandelkow, E. (2016) Tau in physiology and pathology. *Nat. Rev. Neurosci.* **17**, 22–35
12. Hanger, D. P., Anderton, B. H., and Noble, W. (2009) Tau phosphorylation: the therapeutic challenge for neurodegenerative disease. *Trends Mol. Med.* **15**, 112–119
13. Wegmann, S., Biernat, J., and Mandelkow, E. (2021) A current view on Tau protein phosphorylation in Alzheimer's disease. *Curr. Opin. Neurobiol.* **69**, 131–138
14. Martin, L., Latypova, X., Wilson, C. M., Magnaudeix, A., Perrin, M.-L., Yardin, C., *et al*. (2013) Tau protein kinases: involvement in Alzheimer's disease. *Ageing Res. Rev.* **12**, 289–309
15. Wesseling, H., Mair, W., Kumar, M., Schlaffner, C. N., Tang, S., Beerepoot, P., *et al*. (2020) Tau PTM profiles identify patient Heterogeneity and stages of Alzheimer's disease. *Cell* **183**, 1699–1713.e13
16. Pluta, R., and Ułamek-Kozioł, M. (2020) Tau protein-targeted therapies in Alzheimer's disease: current state and future perspectives. In: Huang, X., ed. *Alzheimer's Disease: Drug Discovery*, Exon Publications, Brisbane (AU): 69–82
17. Xiao, Y., and Wang, Y. (2016) Global discovery of protein kinases and other nucleotide-binding proteins by mass spectrometry. *Mass Spectrom. Rev.* **35**, 601–619
18. Ji, J. H., Hwang, H. I., Lee, H. J., Hyun, S. Y., Kang, H. J., and Jang, Y. J. (2010) Purification and proteomic identification of putative upstream regulators of polo-like kinase-1 from mitotic cell extracts. *FEBS Lett.* **584**, 4299–4305
19. Cavallini, A., Brewerton, S., Bell, A., Sargent, S., Glover, S., Hardy, C., *et al*. (2013) An unbiased approach to identifying tau kinases that phosphorylate tau at sites associated with alzheimer disease. *J. Biol. Chem.* **288**, 23331–23347
20. Zeng, L., Wang, W.-H., Arrington, J., Shao, G., Geahlen, R. L., Hu, C.-D., *et al*. (2017) Identification of upstream kinases by fluorescence complementation mass spectrometry. *ACS Cent. Sci.* **3**, 1078–1085
21. Kodama*, Y., and Hu, C.-D. (2010) An improved bimolecular fluorescence complementation assay with a high signal-to-noise ratio. *BioTechniques* **49**, 793–805
22. Tyanova, S., and Cox, J. (2018) Perseus: a bioinformatics platform for integrative analysis of proteomics data in cancer research. *Met. Mol. Biol.* **1711**, 133–148
23. Tyanova, S., Temu, T., Sinitcyn, P., Carlson, A., Hein, M. Y., Geiger, T., *et al*. (2016) The Perseus computational platform for comprehensive analysis of (prote)omics data. *Nat. Met.* **13**, 731–740
24. Szklarczyk, D., Franceschini, A., Wyder, S., Forslund, K., Heller, D., Huerta-Cepas, J., *et al*. (2015) STRING v10: protein-protein interaction networks, integrated over the tree of life. *Nucl. Acids Res.* **43**, D447–D452
25. Iliuk, A. B., Martin, V. A., Alicie, B. M., Geahlen, R. L., and Tao, W. A. (2010) In-depth analyses of kinase-dependent tyrosine phosphoproteomes based on metal ion-functionalized soluble nanopolymers. *Mol. Cell Proteomics* **9**, 2162–2172
26. Yang, X., Boehm, J. S., Yang, X., Salehi-Ashtiani, K., Hao, T., Shen, Y., *et al*. (2011) A public genome-scale lentiviral expression library of human ORFs. *Nat. Met.* **8**, 659–661
27. Johannessen, C. M., Boehm, J. S., Kim, S. Y., Thomas, S. R., Wardwell, L., Johnson, L. A., *et al*. (2010) COT drives resistance to RAF inhibition through MAP kinase pathway reactivation. *Nature* **468**, 968–972
28. Rothbauer, U., Zolghadr, K., Muyldermans, S., Schepers, A., Cardoso, M. C., and Leonhardt, H. (2008) A versatile nanotrap for biochemical and functional studies with fluorescent fusion proteins. *Mol. Cell Proteomics* **7**, 282–289
29. Tudor, C. O., Arighi, C. N., Wang, Q., Wu, C. H., and Vijay-Shanker, K. (2012) The eFIP system for text mining of protein interaction networks of phosphorylated proteins. *Database* **2012**, bas044
30. Arighi, C. N., Siu, A. Y., Tudor, C. O., Nchoutmboube, J. A., Wu, C. H., and Shanker, V. K. (2011) eFIP: a tool for mining functional impact of phosphorylation from literature. *Met. Mol. Biol.* **694**, 63–75
31. Torii, M., Arighi, C. N., Li, G., Wang, Q., Wu, C. H., and Vijay-Shanker, K. (2015) RLIMS-P 2.0: a generalizable rule-based information extraction system for literature mining of protein phosphorylation information. *IEEE/ACM Trans. Comput. Biol. Bioinform.* **12**, 17–29
32. Huang, H., Arighi, C. N., Ross, K. E., Ren, J., Li, G., Chen, S.-C., *et al*. (2018) iPTMnet: an integrated resource for protein post-translational modification network discovery. *Nucl. Acids Res.* **46**, D542–D550
33. Ross, K. E., Huang, H., Ren, J., Arighi, C. N., Li, G., Tudor, C. O., *et al*. (2017) iPTMnet: integrative bioinformatics for studying PTM networks. *Met. Mol. Biol. (Clifton, N.J.)* **1558**, 333–353
34. Tagliabracci, V. S., Wiley, S. E., Guo, X., Kinch, L. N., Durrant, E., Wen, J., *et al*. (2015) A single kinase generates the majority of the secreted phosphoproteome. *Cell* **161**, 1619–1632
35. Mellacheruvu, D., Wright, Z., Couzens, A. L., Lambert, J.-P., St-Denis, N. A., Li, T., *et al*. (2013) The CRAPome: a contaminant repository for affinity purification–mass spectrometry data. *Nat. Met.* **10**, 730–736
36. Manning, G. (2002) The protein kinase complement of the human genome. *Science* **298**, 1912–1934
37. Eid, S., Turk, S., Volkamer, A., Rippmann, F., and Fulle, S. (2017) Kinmap: a web-based tool for interactive navigation through human kinome data. *BMC Bioinform.* **18**, 1–6
38. Uhlen, M., Fagerberg, L., Hallstrom, B. M., Lindskog, C., Oksvold, P., Mardinoglu, A., *et al*. (2015) Tissue-based map of the human proteome. *Science* **347**, 1260419
39. Sjostedt, E., Zhong, W., Fagerberg, L., Karlsson, M., Mitsios, N., Adori, C., *et al*. (2020) An atlas of the protein-coding genes in the human, pig, and mouse brain. *Science* **367**, eaay5947
40. Bai, B., Wang, X., Li, Y., Chen, P.-C., Yu, K., Dey, K. K., *et al*. (2020) Deep multilayer brain proteomics identifies molecular networks in Alzheimer's disease progression. *Neuron* **105**, 975–991.e977
41. [preprint] Morshed, N., Lee, M., Rodriguez, F. H., Lauffenburger, D. A., Mastroeni, D., and White, F. (2020) Quantitative phosphoproteomics uncovers dysregulated kinase networks in Alzheimer's disease. *bioRxiv*. https://doi.org/10.1101/2020.08.18.255778

42. Buljan, M., Ciuffa, R., van Drogen, A., Vichalkovski, A., Mehnert, M., Rosenberger, G., *et al*. (2020) Kinase interaction network expands functional and disease roles of human kinases. *Mol. Cell* **79**, 504–520.e509
43. Szklarczyk, D., Gable, A. L., Nastou, K. C., Lyon, D., Kirsch, R., Pyysalo, S., *et al*. (2021) The STRING database in 2021: customizable protein-protein networks, and functional characterization of user-uploaded gene/measurement sets. *Nucl. Acids Res.* **49**, D605–D612
44. Drummond, E., Pires, G., MacMurray, C., Askenazi, M., Nayak, S., Bourdon, M., *et al*. (2020) Phosphorylated tau interactome in the human Alzheimer's disease brain. *Brain* **143**, 2803–2817
45. Kampers, T., Friedhoff, P., Biernat, J., Mandelkow, E. M., and Mandelkow, E. (1996) RNA stimulates aggregation of microtubule-associated protein tau into Alzheimer-like paired helical filaments. *FEBS Lett.* **399**, 344–349
46. Loomis, P. A., Howard, T. H., Castleberry, R. P., and Binder, L. I. (1990) Identification of nuclear tau isoforms in human neuroblastoma cells. *Proc. Natl. Acad. Sci. U. S. A.* **87**, 8422–8426
47. Sultan, A., Nesslany, F., Violet, M., Bgard, S., Loyens, A., Talahari, S., *et al*. (2011) Nuclear Tau, a key player in neuronal DNA protection. *J. Biol. Chem.* **286**, 4566–4575
48. Qi, H., Cantrelle, F. X., Benhelli-Mokrani, H., Smet-Nocca, C., Buee, L., Lippens, G., *et al*. (2015) Nuclear magnetic resonance spectroscopy characterization of interaction of Tau with DNA and its regulation by phosphorylation. *Biochemistry* **54**, 1525–1533
49. Chirita, C. N., Congdon, E. E., Yin, H., and Kuret, J. (2005) Triggers of full-length tau aggregation: a role for partially folded intermediates. *Biochemistry* **44**, 5862–5872
50. Elbaum-Garfinkle, S., Ramlall, T., and Rhoades, E. (2010) The role of the lipid bilayer in tau aggregation. *Biophys. J.* **98**, 2722–2730
51. Wilson, D. M., and Binder, L. I. (1997) Free fatty acids stimulate the polymerization of tau and amyloid beta peptides. *In vitro* evidence for a common effector of pathogenesis in Alzheimer's disease. *Am. J. Pathol.* **150**, 2181–2195
52. Karikari, T. K., Turner, A., Stass, R., Lee, L. C. Y., Wilson, B., Nagel, D. A., *et al*. (2017) Expression and purification of tau protein and its frontotemporal dementia variants using a cleavable histidine tag. *Protein Expr. Purif.* **130**, 44–54
53. Tepper, K., Biernat, J., Kumar, S., Wegmann, S., Timm, T., Hubschmann, S., *et al*. (2014) Oligomer formation of tau protein hyperphosphorylated in cells. *J. Biol. Chem.* **289**, 34389–34407
54. Mair, W., Muntel, J., Tepper, K., Tang, S., Biernat, J., Seeley, W. W., *et al*. (2016) FLEXITau: quantifying post-translational modifications of tau protein *in vitro* and in human disease. *Anal. Chem.* **88**, 3704–3714
55. Iliuk, A., Liu, X. S., Xue, L., Liu, X., and Tao, W. A. (2012) Chemical visualization of phosphoproteomes on membrane. *Mol. Cell Proteomics* **11**, 629–639
56. Iliuk, A., Martinez, J. S., Hall, M. C., and Tao, W. A. (2011) Phosphorylation assay based on multifunctionalized soluble nanopolymer. *Anal. Chem.* **83**, 2767–2774
57. Iliuk, A. B., and Tao, W. A. (2015) Universal non-antibody detection of protein phosphorylation using pIMAGO. *Curr. Protoc. Chem. Biol.* **7**, 17–25
58. Pan, L., Iliuk, A., Yu, S., Geahlen, R. L., and Tao, W. A. (2012) Multiplexed quantitation of protein expression and phosphorylation based on functionalized soluble nanopolymers. *J. Am. Chem. Soc.* **134**, 18201–18204
59. Glickman, J. F. (2004) Assay development for protein kinase enzymes. In: Markossian, S., Grossman, A., Brimacombe, K., Arkin, M., Auld, D., Austin, C., *et al*., eds. *Assay Guidance Manual*, Eli Lilly & Company and the National Center for Advancing Translational Sciences. Bethesda (MD)
60. Shin, J.-Y., Yu, S.-B., Yu, U.-Y., Ahnjo, S.-M., and Ahn, J.-H. (2010) Swedish mutation within amyloid precursor protein modulates global gene expression towards the pathogenesis of Alzheimer's disease. *BMB Rep.* **43**, 704–709
61. Sung, H. Y., Choi, E. N., Ahn Jo, S., Oh, S., and Ahn, J. H. (2011) Amyloid protein-mediated differential DNA methylation status regulates gene expression in Alzheimer's disease model cell line. *Biochem. Biophys. Res. Commun.* **414**, 700–705
62. Sung, H. Y., Choi, E. N., Lyu, D., Mook-Jung, I., and Ahn, J. H. (2014) Amyloid beta-mediated epigenetic alteration of insulin-like growth factor binding protein 3 controls cell survival in Alzheimer's Disease. *PLoS One* **9**, 1–11
63. Eitan, E., Hutchison, E. R., Marosi, K., Comotto, J., Mustapic, M., Nigam, S. M., *et al*. (2016) Extracellular vesicle-associated A$beta$ mediates trans-neuronal bioenergetic and Ca2+-Handling deficits in alzheimer's disease models. *NPJ Aging Mech. Dis.* **2**, 16019
64. Pandini, G., Pace, V., Copani, A., Squatrito, S., Milardi, D., and Vigneri, R. (2013) Insulin has multiple antiamyloidogenic effects on human neuronal cells. *Endocrinology* **154**, 375–387
65. Tamari, M., Daigo, Y., and Nakamura, Y. (1999) Isolation and characterization of a novel serine threonine kinase gene on chromosome 3p22-21.3. *J. Hum. Genet.* **44**, 116–120
66. Chen, W., Yazicioglu, M., and Cobb, M. H. (2004) Characterization of OSR1, a member of the mammalian ste20p/germinal center kinase subfamily. *J. Biol. Chem.* **279**, 11129–11136
67. Stoothoff, W. H., and Johnson, G. V. W. (2001) Hyperosmotic stress-induced apoptosis and Tau phosphorylation in human neuroblastoma cells. *J. Neurosci. Res.* **65**, 573–582
68. Hahr, J. Y. (2015) Physiology of the Alzheimer's disease. *Med. Hypotheses* **85**, 944–946
69. Allen, M., Carrasquillo, M. M., Funk, C., Heavner, B. D., Zou, F., Younkin, C. S., *et al*. (2016) Human whole genome genotype and transcriptome data for Alzheimer's and other neurodegenerative diseases. *Sci. Data* **3**, 160089
70. Drewes, G., Trinczek, B., Illenberger, S., Biernat, J., Schmitt-Ulms, G., Meyer, H. E., *et al*. (1995) Microtubule-associated protein/microtubule affinity-regulating kinase (p110mark). A novel protein kinase that regulates tau-microtubule interactions and dynamic instability by phosphorylation at the Alzheimer-specific site serine 262. *J. Biol. Chem.* **270**, 7679–7688
71. Liu, F., Liang, Z., Shi, J., Yin, D., El-Akkad, E., Grundke-Iqbal, I., *et al*. (2006) PKA modulates GSK-3beta- and cdk5-catalyzed phosphorylation of tau in site- and kinase-specific manners. *FEBS Lett.* **580**, 6269–6274
72. Farag, A. K., and Roh, E. J. (2019) Death-associated protein kinase (DAPK) family modulators: current and future therapeutic outcomes. *Med. Res. Rev.* **39**, 349–385
73. Oddo, S. (2012) The role of mTOR signaling in Alzheimer disease. *Front. Biosci. (Schol Ed.* **4**, 941–952
74. Obulesu, M., and Lakshmi, M. J. (2014) Apoptosis in alzheimer's disease: an understanding of the physiology, pathology and therapeutic avenues. *Neurochem. Res.* **39**, 2301–2312
75. Zare-Shahabadi, A., Masliah, E., Johnson, G. V. W., and Rezaei, N. (2015) Autophagy in Alzheimer's disease. *Rev. Neurosci.* **26**, 385–395
76. Duan, D. X., Chai, G. S., Ni, Z. F., Hu, Y., Luo, Y., Cheng, X. S., *et al*. (2013) Phosphorylation of tau by death-associated protein kinase 1 antagonizes the kinase-induced cell apoptosis. *J. Alzheimer's Dis.* **37**, 795–808
77. Kyoung Pyo, H., Lovati, E., Pasinetti, G. M., and Ksiezak-Reding, H. (2004) Phosphorylation of tau at THR212 and SER214 in human neuronal and glial cultures: the role of AKT. *Neuroscience* **127**, 649–658
78. Kim, I., Park, E. J., Seo, J., Ko, S. J., Lee, J., and Kim, C. H. (2011) Zinc stimulates tau S214 phosphorylation by the activation of Raf/mitogen-activated protein kinase-kinase/extracellular signal-regulated kinase pathway. *Neuroreport* **22**, 839–844
79. Barbier, P., Zejneli, O., Martinho, M., Lasorsa, A., Belle, V., Smet-Nocca, C., *et al*. (2019) Role of tau as a microtubule-associated protein: structural and functional aspects. *Front. Aging Neurosci.* **11**, 1–14
80. Latour, S., Chow, L. M. L., and Veillette, A. (1996) Differential intrinsic enzymatic activity of syk and Zap-70 protein-tyrosine kinases. *J. Biol. Chem.* **271**, 22782–22790
81. Paris, D., Ait-Ghezala, G., Bachmeier, C., Laco, G., Beaulieu-Abdelahad, D., Lin, Y., *et al*. (2014) The spleen tyrosine kinase (Syk) regulates Alzheimer amyloid-β production and Tau hyperphosphorylation. *J. Biol. Chem.* **289**, 33927–33944
82. Lebouvier, T., Scales, T. M. E., Hanger, D. P., Geahlen, R. L., Lardeux, B., Reynolds, C. H., *et al*. (2008) The microtubule-associated protein tau is phosphorylated by Syk. *Biochim. Biophys. Acta - Mol. Cell Res.* **1783**, 188–192
83. Schweig, J. E., Yao, H., Coppola, K., Jin, C., Crawford, F., Mullan, M., *et al*. (2019) Spleen tyrosine kinase (SYK) blocks autophagic Tau degradation *in vitro* and *in vivo*. *J. Biol. Chem.* **294**, 13378–13395
84. Ho Kim, J., Franck, J., Kang, T., Heinsen, H., Ravid, R., Ferrer, I., *et al*. (2015) Proteome-wide characterization of signalling interactions in the

hippocampal CA4/DG subfield of patients with Alzheimer's disease. *Sci. Rep.* **5**, 11138
85. Wu, Y., Wu, M., Ming, S., Zhan, X., Hu, S., Li, X., *et al*. (2021) TREM-2 promotes Th1 responses by interacting with the CD3zeta-ZAP70 complex following Mycobacterium tuberculosis infection. *J. Clin. Invest.* **131**, e137407
86. Jendresen, C., Arskog, V., Daws, M. R., and Nilsson, L. N. (2017) The Alzheimer's disease risk factors apolipoprotein E and TREM2 are linked in a receptor signaling pathway. *J. Neuroinflam.* **14**, 59
87. Chong, Y.-P., Mulhern, T. D., and Cheng, H.-C. (2005) C-terminal Src kinase (CSK) and CSK-homologous kinase (CHK)—endogenous negative regulators of Src-family protein kinases. *Growth Factors* **23**, 233–244
88. Puig, B., Santpere, G., and Ferrer, I. (2006) P3-305: C-terminal Src kinase (CSK) is diminished in lipid rafts in alzheimer's disease. *Alzheimer's Demen.* **2**, S465
89. Taniguchi, Y. (2016) The bromodomain and extra-terminal domain (BET) family: functional anatomy of BET paralogous proteins. *Int. J. Mol. Sci.* **17**, 1849
90. Xu, Y., and Vakoc, C. R. (2017) Targeting cancer cells with BET bromodomain inhibitors. *Cold Spring Harb. Perspect. Med.* **7**, a026674
91. Magistri, M., Velmeshev, D., Makhmutova, M., and Patel, P.a. (2016) The BET-bromodomain inhibitor JQ1 reduces inflammation and tau phosphorylation at Ser396 in the brain of the 3xTg model of alzheimer's disease. *Curr. Alzheimer Res.* **13**, 985–995
92. Benito, E., Ramachandran, B., Schroeder, H., Schmidt, G., Urbanke, H., Burkhardt, S., *et al*. (2017) The BET/BRD inhibitor JQ1 improves brain plasticity in WT and APP mice. *Transl. Psych.* **7**, e1239
93. McShea, A., Harris, P. L., Webster, K. R., Wahl, A. F., and Smith, M. A. (1997) Abnormal expression of the cell cycle regulators P16 and CDK4 in Alzheimer's disease. *Am. J. Pathol.* **150**, 1933–1939
94. Sanphui, P., Pramanik, S. K., Chatterjee, N., Moorthi, P., Banerji, B., and Biswas, S. C. (2013) Efficacy of cyclin dependent kinase 4 inhibitors as potent neuroprotective agents against insults relevant to Alzheimer's disease. *PLoS One* **8**, e78842
95. Noble, W., Olm, V., Takata, K., Casey, E., Mary, O., Meyerson, J., *et al*. (2003) Cdk5 is a key factor in tau aggregation and tangle formation *in vivo*. *Neuron* **38**, 555–565
96. Abreha, M. H., Ojelade, S., Dammer, E. B., McEachin, Z. T., Duong, D. M., Gearing, M., *et al*. (2021) TBK1 interacts with tau and enhances neurodegeneration in tauopathy. *J. Biol. Chem.* **296**, 100760
97. Hong, Y., Chan, C. B., Kwon, I. S., Li, X., Song, M., Lee, H. P., *et al*. (2012) SRPK2 phosphorylates tau and mediates the cognitive defects in Alzheimer's disease. *J. Neurosci.* **32**, 17262–17272
98. Liu, H., Sugiura, M., Nava, V. E., Edsall, L. C., Kono, K., Poulton, S., *et al*. (2000) Molecular cloning and functional characterization of a novel mammalian sphingosine kinase type 2 isoform. *J. Biol. Chem.* **275**, 19513–19520
99. Lang, B., Armaos, A., and Tartaglia, G. G. (2019) RNAct: Protein-RNA interaction predictions for model organisms with supporting experimental data. *Nucl. Acids Res.* **47**, D601–D606
100. Vizcaino, J. A., Deutsch, E. W., Wang, R., Csordas, A., Reisinger, F., Rios, D., *et al*. (2014) ProteomeXchange provides globally coordinated proteomics data submission and dissemination. *Nat. Biotechnol.* **32**, 223–226
101. Okuda, S., Watanabe, Y., Moriya, Y., Kawano, S., Yamamoto, T., Matsumoto, M., *et al*. (2017) jPOSTrepo: an international standard data repository for proteomes. *Nucl. Acids Res.* **45**, D1107–D1111